NASA/CR-2005-213905
NIA Report No. 2005-01

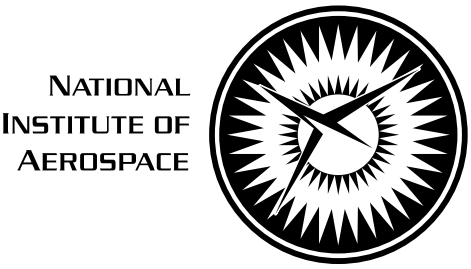

Modeling of Unit-Cells with Z-Pins Using FLASH: Pre-Processing and Post-Processing

Ronald Krueger
National Institute of Aerospace, Hampton, Virginia

August 2005

The NASA STI Program Office . . . in Profile

Since its founding, NASA has been dedicated to the advancement of aeronautics and space science. The NASA Scientific and Technical Information (STI) Program Office plays a key part in helping NASA maintain this important role.

The NASA STI Program Office is operated by Langley Research Center, the lead center for NASA's scientific and technical information. The NASA STI Program Office provides access to the NASA STI Database, the largest collection of aeronautical and space science STI in the world. The Program Office is also NASA's institutional mechanism for disseminating the results of its research and development activities. These results are published by NASA in the NASA STI Report Series, which includes the following report types:

- TECHNICAL PUBLICATION. Reports of completed research or a major significant phase of research that present the results of NASA programs and include extensive data or theoretical analysis. Includes compilations of significant scientific and technical data and information deemed to be of continuing reference value. NASA counterpart of peer-reviewed formal professional papers, but having less stringent limitations on manuscript length and extent of graphic presentations.

- TECHNICAL MEMORANDUM. Scientific and technical findings that are preliminary or of specialized interest, e.g., quick release reports, working papers, and bibliographies that contain minimal annotation. Does not contain extensive analysis.

- CONTRACTOR REPORT. Scientific and technical findings by NASA-sponsored contractors and grantees.

- CONFERENCE PUBLICATION. Collected papers from scientific and technical conferences, symposia, seminars, or other meetings sponsored or co-sponsored by NASA.

- SPECIAL PUBLICATION. Scientific, technical, or historical information from NASA programs, projects, and missions, often concerned with subjects having substantial public interest.

- TECHNICAL TRANSLATION. English-language translations of foreign scientific and technical material pertinent to NASA's mission.

Specialized services that complement the STI Program Office's diverse offerings include creating custom thesauri, building customized databases, organizing and publishing research results ... even providing videos.

For more information about the NASA STI Program Office, see the following:

- Access the NASA STI Program Home Page at ***http://www.sti.nasa.gov***

- E-mail your question via the Internet to help@sti.nasa.gov

- Fax your question to the NASA STI Help Desk at (301) 621-0134

- Phone the NASA STI Help Desk at (301) 621-0390

- Write to:
  NASA STI Help Desk
  NASA Center for AeroSpace Information
  7121 Standard Drive
  Hanover, MD 21076-1320

NASA/CR-2005-213905
NIA Report No. 2005-01

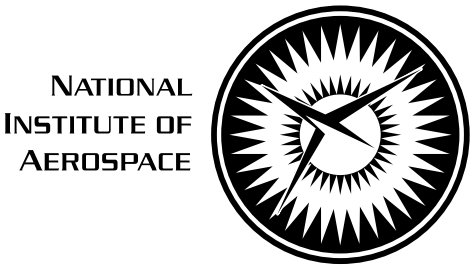

Modeling of Unit-Cells with Z-Pins Using FLASH: Pre-Processing and Post-Processing

Ronald Krueger
National Institute of Aerospace, Hampton, Virginia

National Aeronautics and
Space Administration

Langley Research Center
Hampton, Virginia 23681-2199

Prepared for Langley Research Center
under Contract NAS1-02117

August 2005

Available from:

NASA Center for AeroSpace Information (CASI)
7121 Standard Drive
Hanover, MD 21076-1320
(301) 621-0390

National Technical Information Service (NTIS)
5285 Port Royal Road
Springfield, VA 22161-2171
(703) 605-6000

MODELING OF UNIT-CELLS WITH Z-PINS USING *FLASH:* PRE-PROCESSING AND POST-PROCESSING

Ronald Krueger[1]

ABSTRACT

Although the toughening properties of stitches, z-pins and similar structures have been studied extensively, investigations on the effect of z-pins on the in-plane properties of laminates are limited. A brief summary on the effect of z-pins on the in-plane tensile and compressive properties of composite laminates is presented together with a concise introduction into the finite element code *FLASH*. The remainder of the report illustrates the modeling aspect of unit cells with z-pins in *FLASH* and focuses on input and output data as well as post-processing of results.

LIST OF SYMBOLS

C	length of resin pocket parallel to fiber direction
A_r	fraction of the total reinforced area covered by z-pins
A_Z	cross sectional area of a single z-pin
D_z	z-pin diameter
D_z'	height of z-pin plus resin pocket normal to fiber direction
d	fiber diameter
E_{11}, E_L	Stiffness of lamina parallel to fiber direction
E_{22}, E_T	Stiffness of lamina transverse to fiber direction
E_{Tc}	Compression stiffness of lamina transverse to fiber direction
G	Shear modulus
G_f	Fiber shear modulus
G_{LT}, G_{12}	Lamina shear modulus in principal material directions
G_{sec}	Lamina secant shear modulus
H_z	vertical spacing between z-pins in unit cell
L_z	Horizontal spacing between z-pins in unit cell
n	Ramberg-Osgood curve fitting parameter
N_x, N_y	Axial force resultant on laminate in X,Y direction
N_{xy}	Shear force resultant on laminate in X-Y plane
r_z	areal density of z-pins
u_x, u_y	Displacement in X, Y direction
V_f	Fiber volume fraction
w	kink band width
α	Ramberg-Osgood curve fitting parameter
β	kink band inclination angle
Δx, Δy	distance of fiber misalignment data points in X,Y direction
γ_e	Effective shear strain
γ_s	shear strain

[1] Senior Staff Scientist, National Institute of Aerospace (NIA), 144 Research Drive, Hampton, VA 23666.

γ_p	shear strain
γ_y	Yield strain in shear
λ	loading parameter
ν_{12}	Lamina Poisson's ratio
$\bar{\phi}$	Fiber misalignment angle
σ_c	Strength, critical value of stress
σ_{Ty}	Yield strength in tension
σ_{xx}, σ_{yy}	Normal stress in X, Y direction
σ_{xy}, σ_{yx}	Shear stress in X-Y plane
σ_{ult}	Strength of skin/stiffener-flange laminate
σ_{ultc}	Compression strength of skin/stiffener-flange laminate
σ_{11}, σ_{22}	Normal stress in 1, 2 direction
σ_{12}, σ_{21}	Shear stress in 1-2 plane
τ_e	Effective yield strength in shear
τ_y	Yield strength in shear
τ_{xy}, τ_{yx}	Shear stress in X-Y plane
τ_{12}, τ_{21}	Shear stress in 1-2 plane

1. BACKGROUND

One of the most common failure modes for composite structures is delamination [1-3]. The remote loadings applied to composite components are typically resolved into interlaminar tension and shear stresses at discontinuities that create delaminations under mixed-mode conditions. In the past research has focussed on stitching to increase the delamination resistance of composites [4-8]. More recently z-pins[2] have been proposed to stitch the material together through a combination of friction and adhesion [9-12]. Z-pins are pultruded rods of carbon fiber and epoxy matrix with an approximate diameter of 280 μm or 508 μm. The z-pins are inserted through the thickness of a laminated composite, which is then autoclaved to cure the epoxy as normal. This approach to through-thickness reinforcement offers an alternative to stitching, and can provide much higher areal densities of reinforcement [13].

Examination of the literature shows that the toughening properties of stitches, z-pins and similar structures have been studied extensively, however, investigations on the effect of z-pins on the in-plane properties of laminates are limited [13-17]. Steeves examined the effect of z-pins on the in-plane tensile and compressive properties of composite laminates [13]. Disruption in the alignment of the fibers in a fiber composite leads to a significant reduction in the in-plane compressive strength [18]. Since the diameter of the z-pins (~280 μm) is large relative to the diameter of the fibers (~7 μm) in the composite, the z-pins may cause significant misalignment of the fibers of the composite. A sketch of the typical distribution of fiber misalignment around a z-pin is shown in Figure 1. The z-pin is surrounded by a resin-rich pocket on two sides, caused by the fibers deflecting around the z-pin and leaving a gap in the composite. The maximum misalignment of the deflecting fibers occurs in four locations on the four flanks of the resin-rich pocket.

[2] The generic term z-pin will be used throughout the paper versus the trade mark **Z-Fiber™** registered by Aztex Inc.

Steeves' experiments and numerical finite element simulations using *FLASH* showed that z-pins reduce the in-plane strength of composite laminates. His experimental data from compressive tests showed that the insertion of a field of z-pins into a laminated fiber composite reduces the in-plane compressive strength of the composite by 30% or more. He assumed that the reduction in compressive strength is a consequence of the increased fiber waviness caused by the z-pins [13]. Compression tests within the scanning electron microscope showed that the z-pinned specimens develop microbuckles in the region of greatest fiber waviness around the resin-rich pocket, as would be predicted by the microbuckling model of Budiansky and Fleck [19].

The objective of this report is to present a brief introduction into the finite element code *FLASH* and illustrate the modeling aspect of unit cells with z-pins in *FLASH*. The report focuses on the detailed description of input data for *FLASH* and output obtained from the analysis as well as the post-processing of results. The report is intended to supplement existing user manuals [20, 21]. First, input is described for a finite element model and material data from reference [13]. Second, the correct load input and boundary conditions for compression, tension, shear and combined loading is illustrated. Third, for a composite made of carbon/epoxy modeling for large (0.508 mm diameter) and small (0.28 mm diamter) z-pins is described for 2% and 4% z-pin areal density. Input data are determined for unit cells subjected to five different load cases such as axial compression, combined axial compression and transverse tension, combined axial compression and shear loading as well as combined axial compression, transverse tension and shear loading. Additionally, the output obtained from *FLASH* is explained and separate post-processing options are discussed. The interpretation of the output with respect to the strength of z-pin reinforced lamina is discussed in detail in a separate report [22].

2. INTRODUCTION TO *FLASH*

In order to better assess the influence of critical parameters on lamina compression strength, Fleck and Shu developed a finite element code called *FLASH* [20, 21, 23]. The FE code is based on a 2D general Cosserat couple stress theory that assumes the unidirectional composite lamina is a homogeneous anisotropic material that carries couple stress as well as classical Cauchy point stress [24, 25]. The constitutive response is deduced from a unit cell consisting of a fiber, represented by a linear elastic Timoshenko beam, embedded in a non-linear elastic-plastic matrix [26]. The fiber diameter, d, is the length scale in the constitutive law that controls fiber bending resistance. The continuum theory was implemented within a two-dimensional finite element code that uses 6-noded triangular elements with 3 degrees of freedom at each node (two-displacements and one rotation corresponding to rotation of the fiber cross section). The finite element procedure is based upon a Lagrangian formulation of the finite deformation of the composite and can accommodate both geometric and material non-linearities [23]. The code models finite deformation using a Newton-Raphson incremental solution procedure with a modified Riks algorithm in the final stage to handle snap-back behavior associated with fiber micro-buckling [27]. Boundary loading is piecewise proportional with a loading parameter, λ, for each loading stage [20, 21, 23].

The *FLASH* code assumes micro-buckling initiates from an imperfection in the form of fiber waviness. Inputs include material properties (volume fraction V_f, and stiffness properties

E_L, E_T, E_{Tc}, G_{LT}, G_f, all normalized by the shear yield strength, τ_y) and the Ramberg-Osgood strain hardening law parameters (α, n). *FLASH* allows options for input of fiber misalignment angle due to fiber waviness either as (1) an elliptical patch of waviness, or (2) an arbitrary distribution of initial fiber waviness through initial misalignment angle, $\bar{\phi}$, at the Gauss integration point for each element [20, 21, 23]. The first option prescribes the elliptical patch along one edge of the unit cell. Steeves used the second option to input fiber misalignment distribution obtained from analysis of digital images of specimens taken in a Scanning Electron Microscope (SEM) [13].

3. GENERIC PRE-PROCESSING

3.1 Unit Cell Geometry

The z-pin reinforced composite is divided into unit cells as shown in Figure 2. The size of the unit cell depends on the areal density, r_z (in %) of the z-pins and the diameter of a single z-pin, D_z as shown in Figure 2. The spacing L_z=H_z for a perfect, rectangular z-pin field can be calculated as

$$L_Z = H_Z = \sqrt{\frac{A_Z}{A_r}} \ ,$$

where A_Z is the cross sectional area of a single z-pin

$$A_Z = \frac{\pi D_Z^2}{4}$$

and A_r denotes the fraction of the total reinforced area covered by z-pins

$$A_r = \frac{r_Z}{100} \ .$$

The length of the resin pocket, *C,* may be determined from micrographs of the reinforced laminate as shown in Figure 3.

3.2 Input of Geometrical Points

For the analysis with *FLASH* only one unit cell is modeled as shown in Figure 4. The resin-rich pocket and the z-pin are modeled as voids within the material. Considering axial compression (x-direction) as the driving failure load, modeling a void is justified because the matrix strength and stiffness are low relative to the strength and stiffness of the composite, and the resin-rich pocket can considered to be significantly cracked early in the simulation. Hence, the simulation models the unit cell of a composite including fiber misalignment and internal holes [13]. All meshes generated were composed of six-noded triangular plane-strain elements. The size of the elements

was varied to provide the greatest mesh refinement near the resin pocket, and in the region of greatest fiber misalignment.

First geometric parameters were taken from reference [13]. Since the fiber is completely surrounded by resin the transverse dimension of the modeled void, D'_z, is increased by 0.02 mm compared to the z-pin diameter, D_z as shown in Figure 3a. The finite element code *FLASH* requires the input of geometric data normalized with the fiber diameter of the composite, d as listed in Table 1. Geometrical data for the areas to be meshed is input using the ***GEOMETRICAL POINTS** command in *FLASH*. The coordinates of the points used to create the finite element model of the unit cell with z-pin are printed below and their physical location is sketched in Figure 5.

```
*GEOMETRICAL POINTS
  26
  1              0.00                0.00
  2            125.00                0.00
  3            250.00                0.00
  4              0.00              103.60
  5            125.00              103.60
  6            250.00              103.60
  7            110.00              105.00
  8            140.00              105.00
  9              0.00              124.00
  10            33.00              124.00
  11           217.00              124.00
  12           250.00              124.00
  13            32.00              125.00
  14           217.99              125.00
  15             0.00              126.00
  16            33.00              126.00
  17           217.00              126.00
  18           250.00              126.00
  19           110.00              145.00
  20           140.00              145.00
  21             0.00              146.40
  22           125.00              146.40
  23           250.00              146.40
  24             0.00              250.00
  25           125.00              250.00
  26           250.00              250.00
```

The geometric parameters were used to generate the finite element mesh of the unit cell including the resin-rich pocket as shown in Figure 4.

3.3 Input of Mesh Data

Mesh seed data for the areas to be meshed is input using the **`*MESH SETS`** command in *FLASH*. The input to create 10 mesh sets which form the finite element model of the unit cell with z-pin (see Figure 4) are printed below. The physical location of the mesh sets is sketched in Figure 6.

```
*MESH SETS
  10,6
  1, 1, 4, 2, 2, 5, 8, 10, 0.1, 0.1, 0.1, 0.1
  2, 2, 5, 3, 3, 6, 8, 10, 0.1, 0.1, 10, 10
  4, 4, 9, 5, 7, 10, 8, 10, .25, .25, 0.1, 0.1
  5, 8, 11, 6, 6, 12, 8, 10, .25, .25, 10, 10
  9, 9, 15, 10, 13, 16, 3, 10, 1, 1, 0.1, 0.1
  11, 14, 17, 12, 12, 18, 3, 10, 1, 1, 10, 10
  15, 15, 21, 16, 19, 22, 8, 10, 4, 4, 0.1, 0.1
  17, 20, 22, 18, 18, 23, 8, 10, 4, 4, 10, 10
  21, 21, 24, 22, 22, 25, 8, 10, 10, 10, 0.1, 0.1
  22, 22, 25, 23, 23, 26, 8, 10, 10, 10, 10, 10
```

3.4 Input of Misalignment Data

The finite element code *FLASH* also calls for the input of the fiber misalignment angle [20, 21]. The misalignment angle is input using the **`*MISALIGNMENT TYPE`** and the **`*MISALIGNMENT`** command in *FLASH*. The input used for all analysis is printed below.

```
*MISALIGNMENT TYPE
  2
*MISALIGNMENT
 74,74,3.425,3.425
```

Preliminary analysis with N=1 as input for **`*MISALIGNMENT TYPE`** which was supposed to generate an elliptical patch of waviness was not successful. Post-processing – discussed later - only showed a small band of waviness along the left edge of the specimen (x=0). The waviness in the rest of the specimen was zero. Therefore this approach was abandoned and N=2 was chosen which requires that the discretized misalignment data is provided in a separate input file (**`phiex.dat`**). Input of an arbitrary distribution of the fiber misalignment is possible as by sampling a micrograph as shown in Figure 7 [13]. However, if this information is not available, misalignment angles may be chosen to study the misalignment effect on the reduction of in-plane strength.

To illustrate the input an example is shown in Figure 8 for 10 by 10 sample points on the unit cell which corresponds to a matrix of 10 by 10 data points in the **`phiex.dat`** file. The distance of one point to the adjacent points was set to Δx=26.0 units in x and Δy=26.0 units in y-

direction which extends beyond the unit cell (250 by 250 units) modeled. The distance of points has to be chosen so that the field of data points is larger than the unit cell. The user is advised to check the misalignment input after the execution of **prep** has generated the **flash.inp** file and adjust the distance of adjacent points accordingly. If the misalignment data originates from sampling a micrograph the sample area has to be larger than the model. See reference [21] for details. Only the file named **phiex.dat** will be used during the initial step of the analysis when the file **flash.inp**. is generated during the execution of **prep.**

For the current analyses constant fiber misalignment values of 0°, 1°, 2°, 3°, 4°, 5°, 6°, 7°, 8°, 9°, and 10°, were chosen and 11 **phiex.dat** files were created. Each **phiex.dat** file contains a field of 74 by 74 data points which corresponds to a matrix of 74 by 74 sample points on the unit cell as shown for the example of 5° fiber misalignment.

```
5.000 5.000 5.000 5.000 5.000 5.000 5.000 5.000 5.000 5.000 5.000 5.000
5.000 5.000 5.000 5.000 5.000 5.000 5.000 5.000 5.000 5.000 5.000 5.000
5.000 5.000 5.000 5.000 5.000 5.000 5.000 5.000 5.000 5.000 5.000 5.000
5.000 5.000 5.000 5.000 5.000 5.000 5.000 5.000 5.000 5.000 5.000 5.000
5.000 5.000 5.000 5.000 5.000 5.000 5.000 5.000 5.000 5.000 5.000 5.000
5.000 5.000 5.000 5.000 5.000 5.000 5.000 5.000 5.000 5.000 5.000 5.000
5.000 5.000
5.000 5.000 5.000 5.000 5.000 5.000 …
…
…
```

The distance of one point to the adjacent points was set to 3.425 units in *x* and 3.425 units in *y*-direction to cover the entire unit cell (250 by 250 units).

3.5. Input of Constraints

As mentioned above the composite is divided into unit cells, and only one cell is modeled using periodic boundary conditions. For these models, periodic boundary conditions are prescribed by applying compressive loading symmetrically to the specimen, and constraining three degrees of freedom to prevent rigid body translation and rotation as shown in Figure 9. The constraints are input using the ***TYPE 1 CONSTRAINTS** command in *FLASH*. The input used for all analysis is printed below.

```
*TYPE 1 CONSTRAINTS
  3
  1, 1, 2, 21, 1, 1, 0
  9, 9, 15, 4, 4, 2, 0
  24, 24, 25, 21, 1, 1, 0
```

3.6. Input of Load Data

The loading was input using the **`*STRESS LOADING`** command in *FLASH*. The axial compression stress sketched in Figure 9 is gradually incremented by *FLASH* until it reaches the specified limit defined by the user (σ_{xx}/τ_y =-1000). The limit was deliberately chosen to be well above failure, i.e. formation of kink bands and fiber microbuckling to assure that the analysis reached the failure point and did not terminate at a chosen lower stress [20]. The input used for axial compression loading is printed below.

```
*STRESS LOADING
  10, 1
  1, 1, 4, 1, 1
  -1000, 0, 0, 0, 0
  4, 4, 9, 1, 1
  -1000, 0, 0, 0, 0
  9, 9, 15, 1, 1
  -1000, 0, 0, 0, 0
  15, 15, 21, 1, 1
  -1000, 0, 0, 0, 0
  21, 21, 24, 1, 1
  -1000, 0, 0, 0, 0
  3, 3, 6, 1, 1
  -1000, 0, 0, 0, 0
  6, 6, 12, 1, 1
  -1000, 0, 0, 0, 0
  12, 12, 18, 1, 1
  -1000, 0, 0, 0, 0
  18, 18, 23, 1, 1
  -1000, 0, 0, 0, 0
  23, 23, 26, 1, 1
  -1000, 0, 0, 0, 0
```

3.7. Requests for Output

During the analysis stresses, strains and total fiber alignment angle is written to the file **`flash.out`** after every *N* load steps. The data output request is managed using the **`*OUTPUT FREQUENCY`** commands in *FLASH* as printed below for an output request every 1000 steps.

```
*OUTPUT FREQUENCY
  1000
```

During the analysis, for three boundaries (as shown in Figure 9) data are output to the output file **`post.d`** after each load step. For boundary sections 1 and 2 the net force on each boundary section, resolved along the nominal fiber direction, are given as output. Boundary 3 is a

single node and the displacements of this node are given as output. The data output request is managed using the ***OUTPUT LIST** command in *FLASH* as printed below. The boundary sections selected are shown in Figure 5.

```
*OUTPUT LIST
  3
  1, 1, 4, 1, 1
  1, 1, 4, 1, 1
  1, 1, 4, 1, 1
```

Additionally, the value of the global loading parameter λ is written to the output file at each loading step.

The format of the output files and post-processing of the results is discussed in a separate section below.

3.8. Input of Material Data

The finite element code *FLASH* requires the input of material data normalized with the composite yield shear strength τ_y as given in Table 2 for a generic graphite epoxy material [13]. Additional material parameters used by FLASH are the constants α=0.429 and n=3 in the Ramberg-Osgood strain hardening law, and the fiber volume fraction V_f=0.63 of the composite. The material data is input using the ***MATERIAL CONSTANTS** and ***VFRACTION** commands in FLASH as printed below.

```
*MATERIAL CONSTANTS
  7
  1200, 175, 74, 41, 0.429, 3.0, 87
*VFRACTION
  0.63
```

3.9. Input for a Finite Element Model without Z-Pin

For reference purposes a unit cell without z-pin was modeled and analyzed with FLASH. The mesh with applied load and boundary condition is shown in Figure 10. The geometrical points and the required input data to generate the mesh have been included in Figure 10.

4. PREPROCESSING FOR COMBINED LOADING

For the initial analyses performed, load and boundary conditions were taken from reference [13]. Compressive loading was applied symmetrically to the specimen, and three degrees of freedom were constrained to prevent rigid body translation and rotation as shown in Figure 9.

In general, z-pin reinforced composite structures are subjected to multi axial loads and

input stresses in the unidirectional ply modeled in *FLASH* need to be calculated. For composite plates subjected to external compression and combined compression and shear loading input stresses for *FLASH* were calculated. Using classical laminate theory the external loads were resolved into stresses for the individual plies as shown in Figure 11. Calculated stresses in the critical unidirectional ply consist of axial compression, transverse compression and tension as well as shear stresses. For these combined loading conditions the above mentioned boundary conditions and load input had to be modified.

4.1. FE Models of Z-Pin Unit Cells Subjected to Axial and Transverse Loading

The finite element mesh with load and boundary conditions for axial and transverse compression is shown in Figure 12 with the corresponding input data. Based on results from classical laminate theory mentioned above, the transverse compression load was chosen to be 2% of the compression load applied axially. In order to avoid the collapse of the void under transverse compression points A and B on the periphery of the void could be constrained in transverse direction as shown in Figure 12. In reality, the boundary condition of zero displacements on the periphery of the void is not met due to pin compliance. However, the assumed boundary condition is adopted in order to obtain an estimate for the extreme case of a rigid pin [28]. Nevertheless, analysis without constraints suggested that constraining points A and B for small transverse compression loads leads to overly conservative results.

The finite element mesh with load and boundary conditions for axial compression and transverse tension are shown in Figure 13. As for the previous case the transverse load was chosen to be 2% of the compression load applied axially. For transverse tension it is not required to avoid the collapse of the void.

4.2. FE Models of Z-Pin Unit Cells Subjected to Axial Compression and Shear Loading

The finite element mesh with load and boundary conditions for axial compression combined with shear are shown in Figure 14. Based on results from classical laminate theory mentioned above, the shear load was chosen to be 10% of the compression load applied axially. For the combined axial compression and shear load case it was decided not to prevent the collapse of the void as explained in detail in the appendix of reference 23.

The finite element mesh with load and boundary conditions for axial compression and transverse tension combined with shear are shown in Figure 15. As for the previous case the shear load was chosen to be 10% of the compression load applied axially and the transverse tension load corresponded to 2% of the compression load as discussed in the previous section. For this combined load case it was decided not to prevent the collapse of the void as explained in detail in the appendix of reference 23.

5. UNIT CELL MODELS FOR 2% AND 5% Z-PIN REINFORCEMENT.

For another carbon fiber reinforced epoxy material the data used as input for the analyses with *FLASH* are listed in Table 3. The specimens were reinforced with small z-pins of

D_z=0.279 mm (0.011 in) and large z-pins of D_z=0.508 mm (0.02 in) diameter. Three specimen types were manufactured containing reinforcement fields with r_z=2% areal density for the large z-pin and r_z=2% and r_z=4% areal density for the small z-pins respectively. Geometric data such as z-pin spacing, L_z=H_z, as well as width, D'_z, and length, C, of the resin pocket as defined in Figure 3 was measured from micrographs taken of different specimens. The averaged data used as input for the analysis is summarized in Table 4.

Based on results from classical laminate theory shown in Figure 11 and Table 5, five load cases were considered as input for analysis of the unit cells: A pure axial compression load case, a combined axial compression - 2% transverse tension load case, a combined axial compression - 10% shear load case, a combined axial compression - 50% shear load case, and an axial compression - 2% transverse tension load case combined with 10% shear loading. The input for all five cases is summarized in Table 6.

The finite element meshes are shown in Figures 16, 17, and 18 for the small pin with 2% and 4% areal density and the large pin with 2% areal density. As before the resin-rich pocket and the z-pin are modeled as voids within the material. It is assumed that the fiber is completely surrounded by resin as shown in Figure 3 and therefore the transverse dimension of the modeled void, D'_z, is increased by 0.02 mm compared to the z-pin diameter, D_z. The normalized dimensions required as input were included in the figures as well as the input for the **`*GEOMETRICAL POINTS`** command in *FLASH*. Loads given in Table 6 were applied as discussed in section 4.

6. POSTPROCESSING OF RESULTS

6.1. FLASH Output Files

During the analysis nodal point coordinates, element topology and results are is written to the file **`flash.out`** after every N load steps. The file **`flash.out`** contains a header,

```
1Ccomnew 0.00000E+00            FIBER MICROBUCKLING  3
```

the nodal point coordinates

```
2C
 -1    1 0.00000E+00 0.00000E+00
 -1    2 0.00000E+00 0.15646E+02
 -1    3 0.00000E+00 0.31293E+02
 -1    4 0.00000E+00 0.42553E+02
 -1 …
 -3
```

the element topology

```
3C
 -1    1    8
 -2    1  374  372  155  373  154
```

```
 -1    2    8
 -2    1    3  374    2  156  155
 -1    3    8
 -2  372  710  708  581  709  580
 -1 …
 -3
```

the initial fiber misalignment $\bar{\phi}$

```
-3
  100CLCASE1 0.00000E+00            Fiber Misalignment   3    0
 -4  MISALIGN    1    3    0
 -5  PHIBAR      1    1    1    0    0
 -1    1    8    0    0    6
 -2    1 0.40000E+01
 -2    2 0.40000E+01
 -2    3 0.40000E+01
 -2    4 0.40000E+01
 -2    5 0.40000E+01
 -2    6 0.40000E+01
 -1    2    8    0    0    6
 -2    1 0.40000E+01
 -2    2 0.40000E+01
 -2    3 0.40000E+01
 -2    4 0.40000E+01
 -2 …
 -3
```

the normalized displacements u_x/d and u_y/d at all nodal points

```
100CLCASE1 0.12052E-01            Fiber Microbuckling  3 1000
 -4  DISPLACE    3    1    0
 -5  UX          1    2    1    0    0
 -5  UY          1    2    2    0    0
 -5  U           1    2    0    0    1ALL
 -1    1 0.14712E+01 -0.32663E+01
 -1    2 0.80530E+00 -0.32449E+01
 -1    3 0.14974E+00 -0.31895E+01
 -1    4-0.31371E+00 -0.31129E+01
 -1 …
 -3
```

the normalized stresses σ_{xx}/τ_y, σ_{yy}/τ_y, σ_{xy}/τ_y and σ_{yx}/τ_y, the normalized effective shear stress

τ_e/τ_y, the strains γ_s and γ_p, the fiber misalignment $\bar{\phi}$ and others [20]

```
100CLCASE1 0.12052E-01              Fiber Microbuckling  3 1000
 -4  STRSSTRN   12    3    0
 -5  SIG_XX      1    4    1    1    0
 -5  SIG_YY      1    4    2    2    0
 -5  SIG_XY      1    4    1    2    0
 -5  SIG_YX      1    4    2    1    0
 -5  TAU_E       1    1    2    1    0
 -5  E_LP        1    1    2    1    0
 -5  E_LM        1    1    2    1    0
 -5  E_T         1    1    2    1    0
 -5  GAMA_S      1    1    2    1    0
 -5  KAPPA       1    1    2    1    0
 -5  GAMA_P      1    1    2    1    0
 -5  PHI         1    1    2    1    0
 -1    1    8    0    0    6
 -2 1 -0.12328E+02 0.20839E+00 -0.11766E+00 -0.13105E+00 0.14941E+01 -0.30784E-02
 -2 1 -0.25050E-02 0.17207E-03  0.20919E-01 -0.57344E-03 0.10263E-01  0.76157E+01
 -2 2 -0.11658E+02 0.44093E+00 -0.74204E+00 -0.73252E+00 0.74208E+00 -0.28156E-02
 -2 2 -0.25441E-02 0.18100E-02  0.60815E-02 -0.27141E-03 0.13715E-02  0.66904E+01
 -2 3 -0.13010E+02 0.17288E-01 -0.74737E+00 -0.74508E+00 0.79505E+00 -0.30924E-02
 -2 3 -0.28856E-02 0.63897E-04  0.72372E-02 -0.20685E-03 0.15640E-02  0.67907E+01
 -2 4 -0.11966E+02 0.32614E+00 -0.32097E+00 -0.30034E+00 0.12303E+01 -0.29931E-02
 -2 4 -0.24544E-02 0.11352E-02  0.14406E-01 -0.53866E-03 0.57257E-02  0.72148E+01
 -2 …
 -3
```

During the analysis, data for three boundaries are output to the output file **post.d** The file **post.d** contains contains seven columns. Column 1 lists the load step number, column 2 lists load increase (+1) or decrease (-1), columns 3 and 4 list the normalized displacements u_x/d and u_y/d for the selected node on boundary 3, columns 5 and 6 list the net loads on boundary sections 1 and 2 as shown in Figure 9. Column 7 lists global loading parameter λ for each load step, where λ is a measure of how close the simulation is to fulfilling the requested stress loading discussed in section 3.6.

```
 0  1  0.00000E+00  0.00000E+00  0.00000E+00  0.00000E+00  0.00000E+00
 1  1 -0.24101E-01 -0.13840E-01  0.10106E+03  0.10106E+03  0.96809E-03
 2  1 -0.37684E-01 -0.22066E-01  0.15836E+03  0.15836E+03  0.15167E-02
 3  1 -0.52874E-01 -0.31723E-01  0.22269E+03  0.22269E+03  0.21325E-02
 4  1 -0.69664E-01 -0.43129E-01  0.29416E+03  0.29416E+03  0.28163E-02
…
```

```
 996  1 -0.49693E+00  0.21751E+00  0.19896E+04  0.19896E+04  0.18922E-01
 997  1 -0.49626E+00  0.21723E+00  0.19925E+04  0.19925E+04  0.18949E-01
 998  1 -0.49530E+00  0.21693E+00  0.19966E+04  0.19966E+04  0.18988E-01
 999  1 -0.49464E+00  0.21683E+00  0.19995E+04  0.19995E+04  0.19015E-01
1000  1 -0.49373E+00  0.21680E+00  0.20036E+04  0.20036E+04  0.19053E-01
```

6.2. Result Visualization

The output file **`flash.out`** is formatted to be used with the commercial post-processing software *FEMGV*[3]. A translation routine (**`make_post.f`**) was developed, which reads **`flash.out`** and creates output data of the model (**`flash_pat.out`**) and displacements (**`flash.dis`**) in neutral file format to be used with *PATRAN*[4]. The routine can also create output of the model and result data (**`flash.dat`**) to be used with *Tecplot*[5]. The routine can easily be modified to create an output file in a particular format that is compatible with a graphics package of the user's choice.

6.2.1 Examples of Deformation Plots

The deformed finite element meshes for the unit cell under axial compression are shown in Figure 19. At the beginning of the loading a symmetric deformation with respect to the two axis of symmetry can be observed as shown in Figure 19a. At the edge where the axial compression stress is applied a non-uniform displacement distribution can be observed which forms an axial contraction. The increased displacement is caused by a reduced stiffness which is the result of modeling the resin pocket and z-pin as a void. At the end of the analysis after passing the failure point and the formation of kink bands the deformation grows to be unsymmetrical and the unit cell becomes increasingly distorted as shown in Figure 19b.

The deformed mesh for axial and transverse compression is shown in Figure 20. The transverse compression load was 2% of the compression load applied axially as shown in Figure 12. Analysis without constraints as shown in Figure 20 suggested that constraining points A and B shown in Figure 12, was not required for small transverse compression loads. Compared to the deformation shown in Figure 19a for the pure compression case the axial displacement shown in Figure 20 is reduced at the top and bottom edges where the transverse compression is applied and the void remains open.

The deformed mesh for axial compression and transverse tension are shown in Figure 21. As for the previous case the transverse load was chosen to be 2% of the compression load applied axially as shown in Figure 13. Compared to the deformation for the pure compression case as shown in Figure 19a the axial displacement shown in Figure 21 has increased at the top and bottom edges where the transverse tension stress is applied; also the void opening has increased.

---

[3] http://www.femsys.co.uk/

[4] http://www.mscsoftware.com/products/quick_prod.cfm

[5] http://www.tecplot.com/

6.2.2 Examples of Contour Plots

As an example the contour plots of the fiber misalignment $\bar{\phi}$, the effective shear stress τ_e and the strains γ_s and γ_p, are shown in Figures 24-27 for the unit cell subjected to axial and transverse compression. The contours correspond to the end of the analysis after passing the failure point where the severe color gradients indicate the formation and location of kink bands.

6.2.3 Examples of Stress-Displacement Plots to Obtain Compression Strength

As an example typical stress versus displacements plots are shown in Figures 28 and 29. Typically the `post.d` file is read into a graphing program such as KaleidaGraph™ or Excel™. Here the stress is obtained by multiplying the global loading parameter λ from column (#7) of the output file `post.d` with the matrix yield stress τ_y from the Ramberg-Osgood strain hardening law that is used as input and the requested stress loading (-1000) described in section 3.6. The compression stress $\sigma_{xx}= \lambda\ \tau_y\ 1000$ is plotted versus the normalized displacement in x-direction (u_x/d) for the selected node on boundary 3 as shown in Figure 9. The normalized displacement (u_x/d) is listed in column (#3) of the output file `post.d`. As shown in Figures 28 and 29, the plot typically indicates a clear first maximum. The exact maximum value, which is the predicted compression strength, is best found in the data rather than the plot.

ACKNOWLEDGEMENTS.

This research was supported and partially funded by Sikorsky Aircraft and the Aviation Applied Technology Directorate under Technology Investment Agreement No. DAAH10-02-2-0001 as part of the Survivable – Affordable - Repairable – Airframe - Program (SARAP).

The author gratefully acknowledge Prof. Noman A. Fleck of University of Cambridge, United Kingdom and Dr. Craig A. Steeves of Princeton University for providing the FLASH finite element code and insight into its use and application.

REFERENCES

[1] T.K. O'Brien, *Fracture Mechanics of Composite Delamination*, in ASM Handbook, Volume 21, Composites: ASM International, 2001, pp. 241-245.

[2] V.V. Bolotin, *Delaminations in composite structures: its origin, buckling, growth and stability*, Composites Part B: Engineering, vol. 27B, pp. 129--145, 1996.

[3] T.E. Tay, *Characterization and analysis of delamination fracture in composites - An overview of developments from 1990 to 2001*, Applied Mechanics Reviews, vol. 56, pp. 1-32, 2003.

[4] L.K. Jain, K.A. Dransfield, and Y.-W. Mai, *On the effect of stitching in CFRPs - II: mode II delamination toughness*, Composites Science and Techonology, vol. 58, pp. 829-837, 1998.

[5] K.A. Dransfield, L.K. Jain, and Y.-W. Mai, *On the effect of stitching in CFRPs - I: mode I delamination toughness*, Composites Science and Technology, vol. 58, pp. 815-827, 1998.

[6] D. Shu and Y.-W. Mai., *Effect of stitching on interlaminar delamination extension in composite laminates*, Composites Science and Technology, vol. 49, pp. 165-171, 1993.

[7] L.K. Jain and Y.-W. Mai., *Determination of mode II delamination toughness in stitched laminated composites*, Composites Science and Techonology, vol. 55, pp. 241-253, 1995.

[8] B.N. Cox, *Constitutive model for a fibre tow bridging a delamination crack.*, Mechanics of Composite Structures and Materials, vol. 6, pp. 117-138, 1999.
[9] D. Cartie and I. Partridge., *Z-pinned composite laminates: Improvements in delamination resistance*, presented at 5th International Conference on Deformation and Fracture of Composites, 1999.
[10] G. Freitas, T. Fusco, T. Campbell, J. Harris, and R. S., *Z-fiber technology and products for enhancing composite design.*, presented at AGARD Conference Proceedings 590: Bolted/Bonded Joints in Polymeric Composites, 1996.
[11] B. Budiansky and J.C. Amazigo, *Toughening by aligned, frictionally constrained fibers*, Journal of Mechanics and Physics of Solids, vol. 37, pp. 93-109, 1989.
[12] J.D. Barrett, *The mechanics of z-fiber reinforcement*, Composite Structures, vol. 36, pp. 23-32, 1996.
[13] C.A. Steeves, *Mechanics of Failure in Composite Structures*, in Department of Engineering. Cambridge, United Kingdom: University of Cambridge, 2001.
[14] R. Massabo and B.N. Cox, *Unusual Characteristics of Mixed-Mode Delamination Fracture in the Presence of Large-Scale Bridging*, Mechanics of Composite Materials and Structures, 8:61–80, 2001, vol. 8, pp. 61-80, 2001.
[15] K.L. Rugg, B.N. Cox, and R. Massabò, *Mixed mode delamination of polymer composite laminates reinforced through the thickness by Z-fibers.*, Composites A: applied science and manufacturing, vol. 33, pp. 177–190, 2002.
[16] M. He and B.N. Cox, *Crack bridging by through-thickness reinforcement in delaminating curved structures*, Composites Part A: Applied Science and Manufacturing, vol. 29, pp. 377-393, 1998.
[17] R. Massabo and B.N. Cox, *Concepts for bridged Mode ii delamination cracks*, Journal of the Mechanics and Physics of Solids, vol. 47, pp. 1265-1300, 1997.
[18] N.A. Fleck, *Compressive failure in fiber composites*, Advances in Applied Mechanics, vol. 33, pp. 43-117, 1997.
[19] B. Budiansky and N.A. Fleck., *Compressive failure of fibre composites*, Journal of Mechanics and Physics of Solids, vol. 41, pp. 183-211, 1993.
[20] J.Y. Shu and N.A. Fleck., *User's manual for finite element code for fibre microbuckling. Technical Report CUED/C-MATS/TR.224*, University of Cambridge Department of Engineering. 1995.
[21] D. Liu and N.A. Fleck., *User's manual II for finite element code FLASH for fibre microbuckling,Technical Report CUED/C-MICROMECH/TR.29*, Cambridge University, Engineering Department 1999.
[22] T.K. O'Brien, R. Krueger, and J. Schaff, *Influence of compression and shear on the strength of composite laminates with Z-pinned reinforcement*, NASA Langley Research Center, Hampton, VA, NASA/TM-2005-XXXXX, 2005.
[23] N.A. Fleck and J.Y. Shu, *Microbuckle initiation in fibre composites: a finite element study*, Journal of Mechanics and Physics of Solids, vol. 43, pp. 1887-1918, 1995.
[24] E. Cosserat and F. Cosserat, *Theorie des Corps Deformables*. Paris.: Herman et fils, 1909.
[25] W.T. Koiter, *Couple stresses in the theory of elasticity, I and II.*, Proc. Ned. Akad. Wet., vol. 67, pp. 17-44, 1964.
[26] S.P. Timoshenko and J.N. Goodier, *Theory of Elasticity*, 3rd ed: McGraw-Hill, 1970.
[27] M.A. Crisfield, *Non-linear Finite Element Analysis of Solids and Structures*, vol. 1, chapter 9: John Wiley & Sons, U.K., 1991.
[28] N.A. Fleck, D. Liu, and J.Y. Shu, *Microbuckle initiation from a hole and from the free edge of a fibre composite*, International Journal of Solids and Structures, vol. 37, pp. 2757-2775, 2000.

LIST OF TABLES

Table 1.

Dimensions of Unit Cell

Graphite/Epoxy UD Prepreg with 2% Z-Pins [13]		
	from	normalized with d_f
D_Z	0.28 mm	
D'_Z	0.3 mm	42.8
H_Z	1.75 mm	250
L_Z	1.75 mm	250
C	1.29 mm	184
d	7 μm	1

Table 2**.**

Material Properties for Initial Preliminary Analysis

Graphite/Epoxy Prepreg (A) [13]		
	from	normalized with τ_{xy}
E_{11}	117 GPa	1083
E_{22} (tension)	9.0 GPa	83.33
E_{22} (compression)	9.5 GPa	87.96
G_{12}	4.8 GPa	44.44
G_{f}	22 GPa	203.7
τ_{y}	108 MPa	1
d	7 μm	-
V_{f}	0.55	-
α	3/7	-
n	3	-
Generic Graphite/Epoxy Prepreg (B) [13]		
		normalized with τ_{xy}
E_{11}	-	1200
E_{22} (tension)	-	74
E_{22} (compression)	-	87
G_{12}	-	41
G_{f}	-	175
τ_{y}	-	-
d	7 μm	-
V_{f}	0.63	-
α	0.429	-
n	3	-

Table 3.

Carbon/Epoxy Material Properties

Graphite/Epoxy UD Prepreg		
	from	normalized with τ_{xy}
E_{11}	161 GPa	4248
E_{22} (tension)	11.4 GPa	301
E_{22} (compression)	12.8 GPa	338
G_{12}	5.17 GPa	136
G_{f}	22 GPa	580
τ_{y}	37 MPa	1
d	5.1 μm	-
V_{f}	0.59	-
α	0.00923	-
n	8.54	-

Table 4.

Dimensions of Unit Cells

Graphite/Epoxy UD Prepreg with 2% large diameter Z-Pins		
	from	normalized with *d*
D_Z	0.508 mm	-
D'_Z	0.528 mm	103.53
H_Z	3.175 mm	622.55
L_Z	3.175 mm	622.55
C	2.1844 mm	428.31
Graphite/Epoxy UD Prepreg with 4% small diameter Z-Pins		
	from	normalized with *d*
D_Z	0.28 mm	-
D'_Z	0.3 mm	58.8
H_Z	1.2446 mm	244
L_Z	1.2446 mm	244
C	0.868 mm	170.2
Graphite/Epoxy UD Prepreg with 2% small diameter Z-Pins		
	from	normalized with *d*
D_Z	0.28 mm	-
D'_Z	0.3 mm	58.8
H_Z	1.7526 mm	343.65
L_Z	1.7526 mm	343.65
C	0.868 mm	170.2

Table 5.

Load Cases for Laminate Analysis and Results

external load N_x=-1000 lbs/in			
	σ_{11}, psi	σ_{22}, psi	τ_{12}, psi
$[0/90]_s$	-1898	-29.5 (~2% σ_{11})	0
$[0/\pm45]_s$	-2304	+48.9 (~2% σ_{11})	0
$[0/45/-45/90]_s$	-2597	-3.3 (~0.2% σ_{11})	0
external load N_x=-1000 lbs/in, N_{xy}=-1000 lbs/in			
	σ_{11}, psi	σ_{22}, psi	τ_{12}, psi
$[0/90]_s$	-1898	-29.5	-1000 (~50% σ_{11})
$[0/\pm45]_s$	-2304	+48.9 (~2% σ_{11})	-222 (~10% σ_{11})
$[0/45/-45/90]_s$	-2597	-3.3	-275 (~10% σ_{11})

Table 6.

FLASH Input for Load Cases Used for Strength Reduction Analysis

	axial compression	compression/ 2%transverse tension	compression 10% shear	compression 50% shear	compression 2% tension 10% shear
σ_{11}/τ_y	-1000	-1000	-1000	-1000	-1000
σ_{22}/τ_y	-	+20	-	-	+20
τ_{12}/τ_y	-	-	100	500	100
τ_{21}/τ_y	-	-	100	500	100

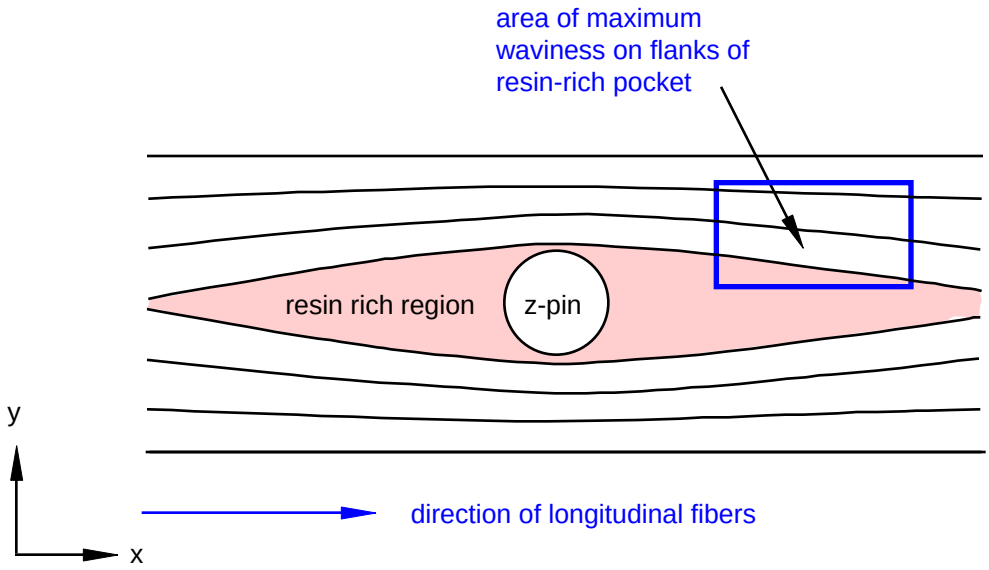

Figure 1: Typical shape of local area around z-pin

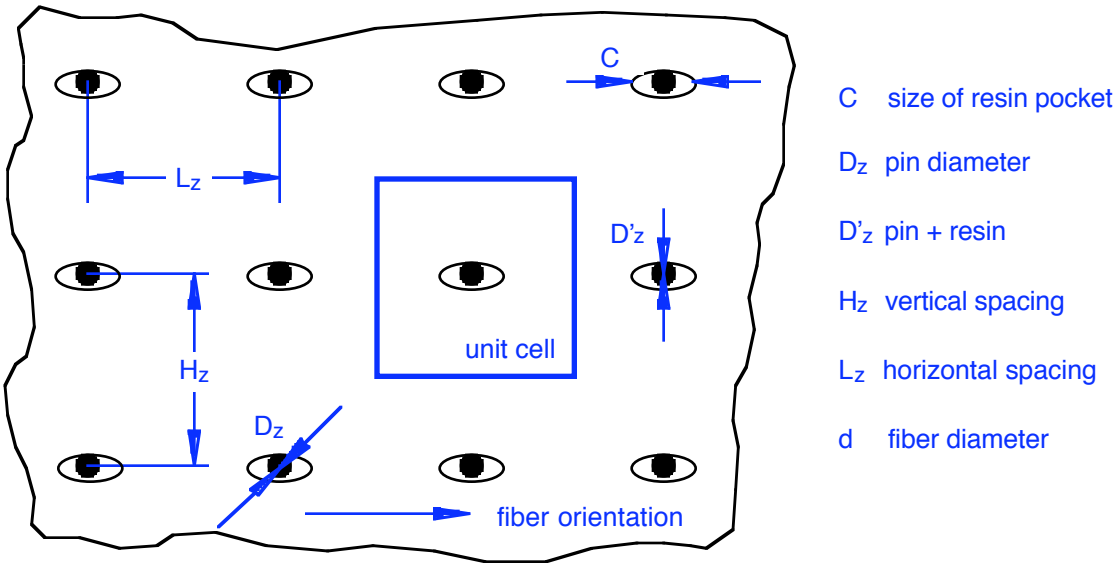

Figure 2: Detail of perfect z-pin field with typical dimensions and unit cell

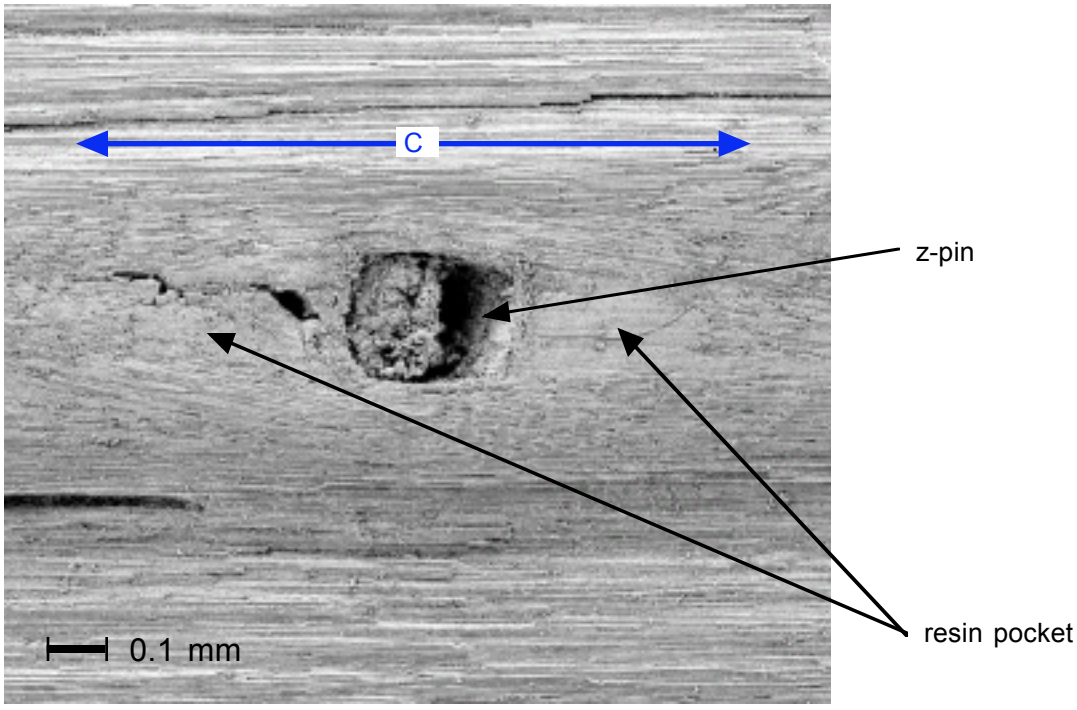

Figure 3: Micrograph of individual z-pin with surrounding laminate [13]

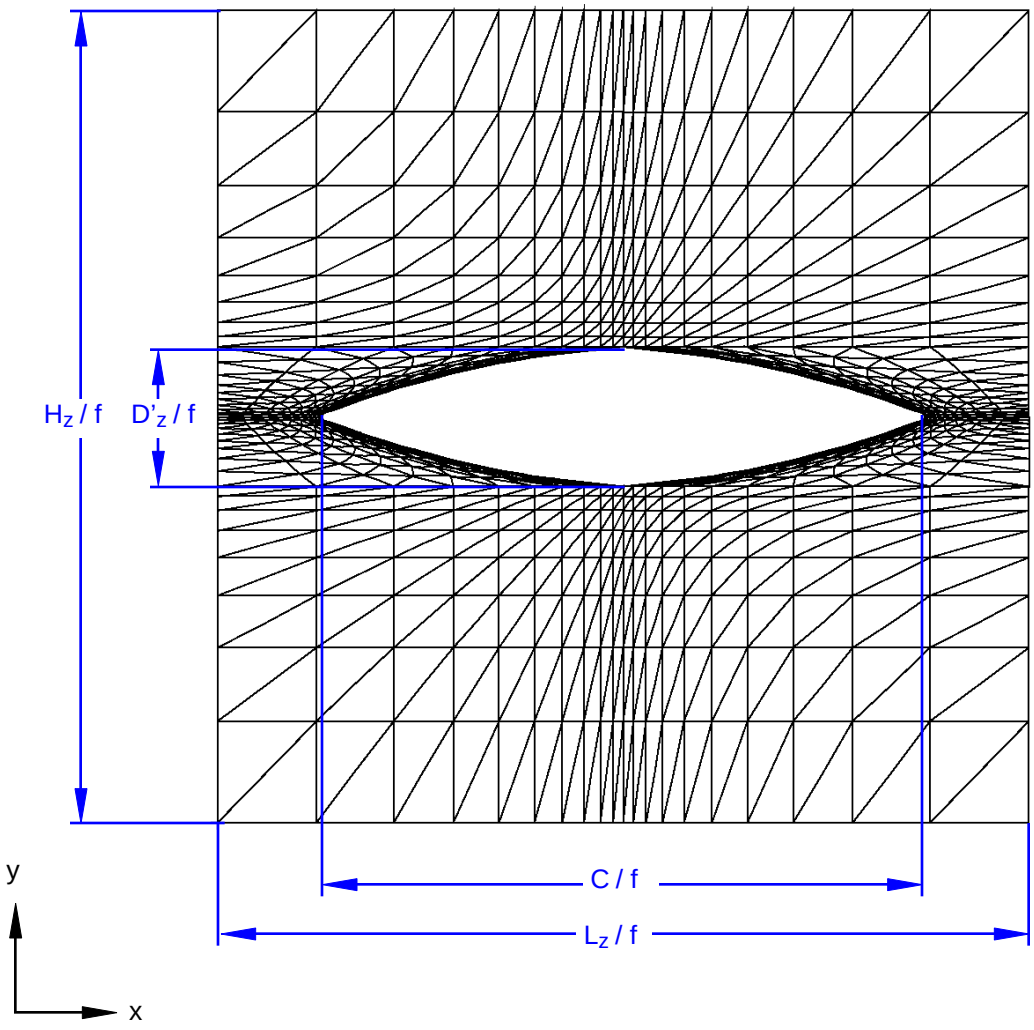

Figure 4: Typical finite element mesh of unit cell with normalized dimensions and initial misalignment due to z-pin insertion

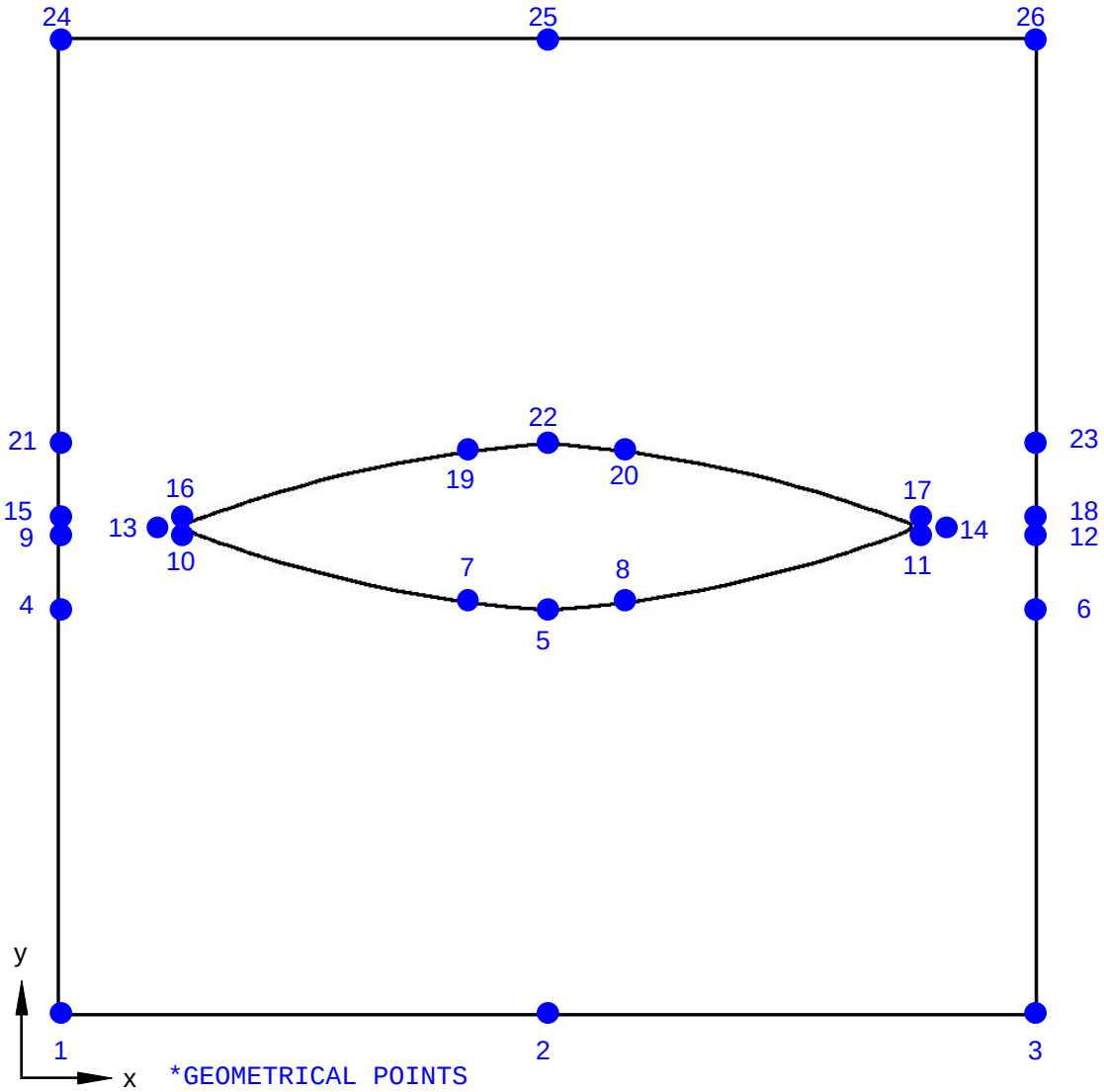


```
*GEOMETRICAL POINTS
  26
  1              0.00                0.00
  2            125.00                0.00
  3            250.00                0.00
  4              0.00              103.60
  5            125.00              103.60
  6            250.00              103.60
  7            110.00              105.00
  8            140.00              105.00
  9              0.00              124.00
  10            33.00              124.00
  11           217.00              124.00
  12           250.00              124.00
  13            32.00              125.00
  14           217.99              125.00
  ...
  ...
  26           250.00              250.00
```

Figure 5: Outline of unit cell and void with geometry points

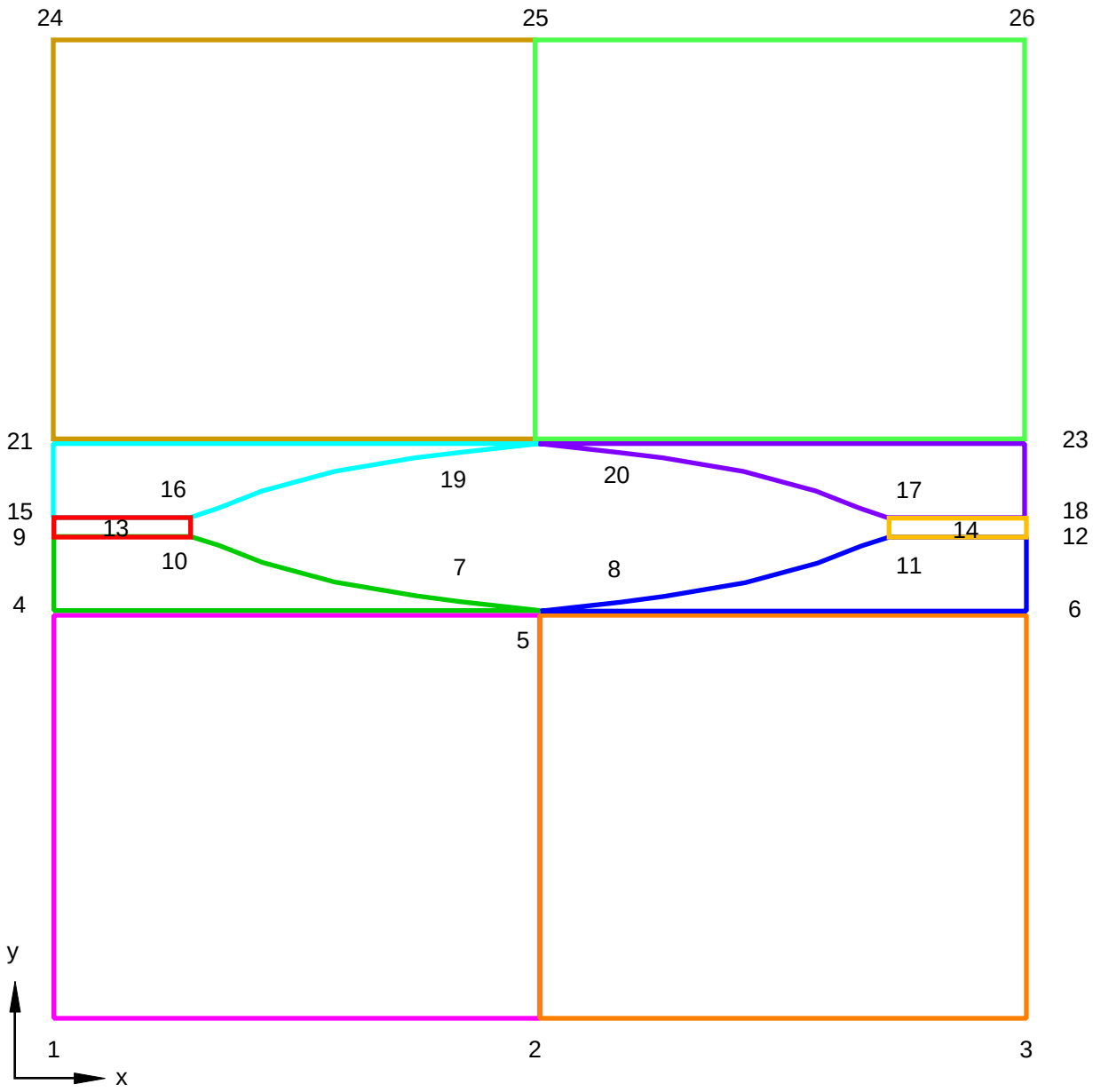


```
*MESH SETS
  10,6
  1, 1, 4, 2, 2, 5, 8, 10, 0.1, 0.1, 0.1, 0.1
  2, 2, 5, 3, 3, 6, 8, 10, 0.1, 0.1, 10, 10
  4, 4, 9, 5, 7, 10, 8, 10, .25, .25, 0.1, 0.1
  5, 8, 11, 6, 6, 12, 8, 10, .25, .25, 10, 10
  9, 9, 15, 10, 13, 16, 3, 10, 1, 1, 0.1, 0.1
  11, 14, 17, 12, 12, 18, 3, 10, 1, 1, 10, 10
  15, 15, 21, 16, 19, 22, 8, 10, 4, 4, 0.1, 0.1
  17, 20, 22, 18, 18, 23, 8, 10, 4, 4, 10, 10
  21, 21, 24, 22, 22, 25, 8, 10, 10, 10, 0.1, 0.1
  22, 22, 25, 23, 23, 26, 8, 10, 10, 10, 10, 10
```

Figure 6: Outline of unit cell and void with geometry points and mesh sets

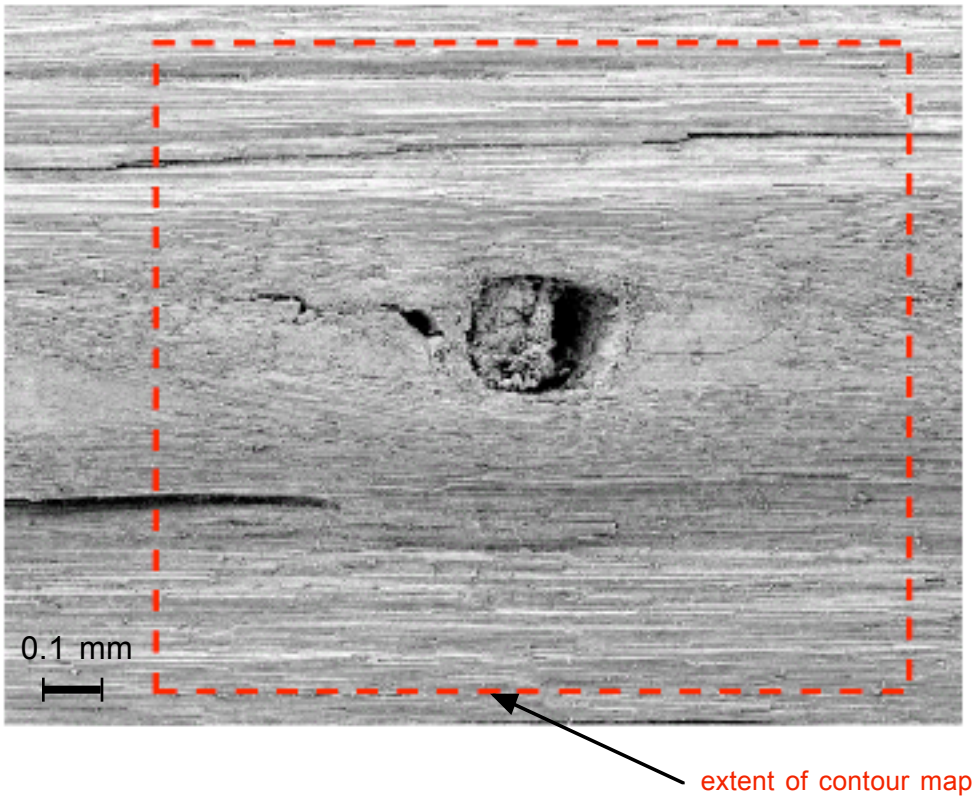

(a). Electron micrograph of individual z-pin with surrounding laminate [13]

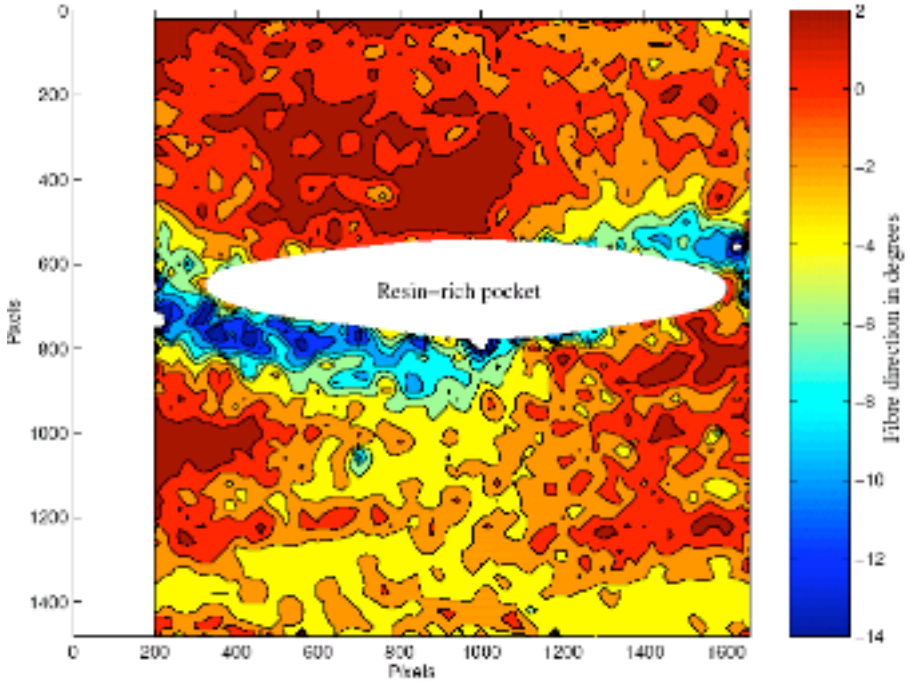

(b). Contour map of fiber alignment angle [13]

Figure 7: Measurement of fiber misalignment angle

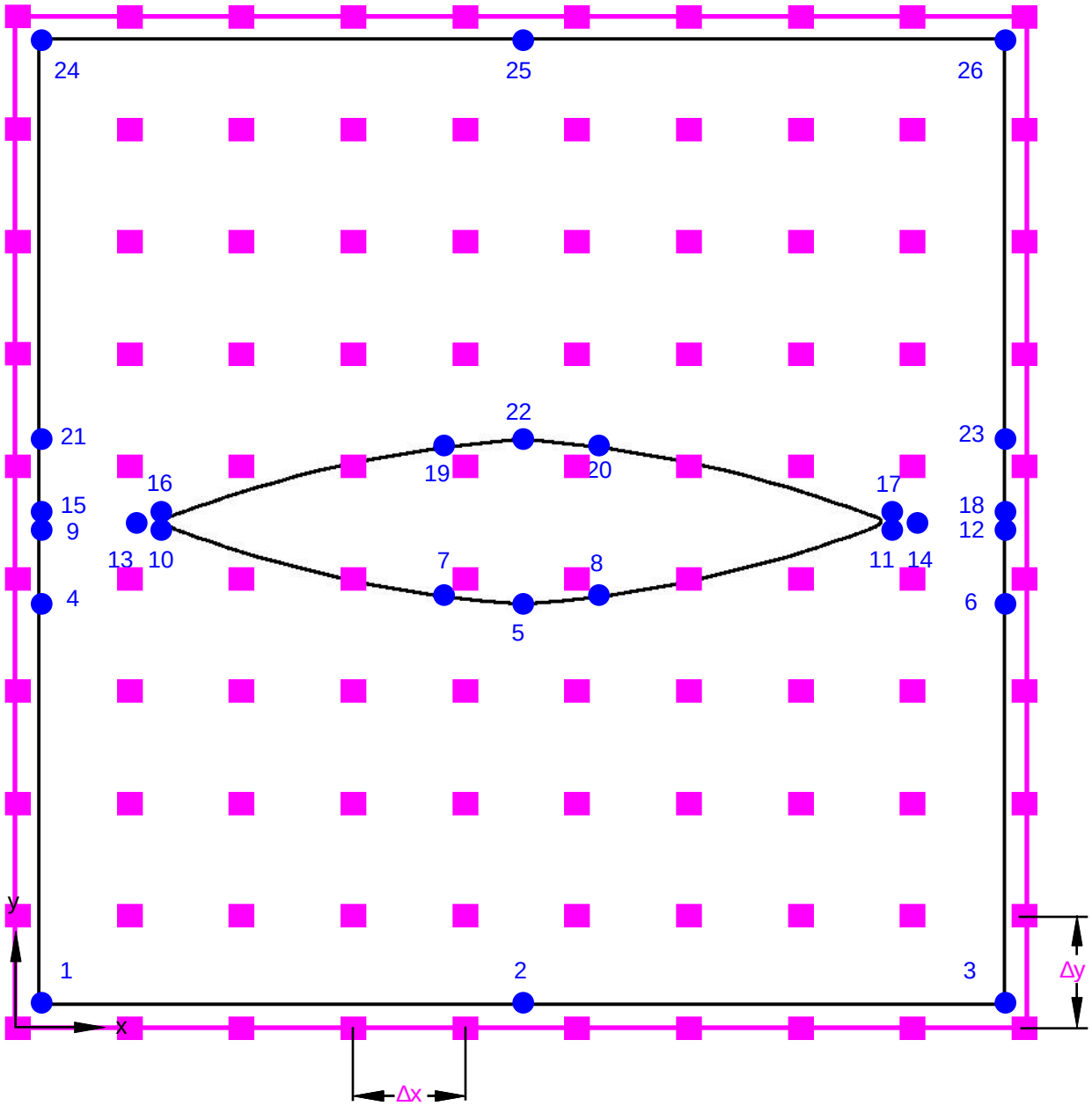


```
*GEOMETRICAL POINTS
  26
  1              0.00              0.00
  2            125.00              0.00
  3            250.00              0.00
  4              0.00            103.60
  5            125.00            103.60
  6            250.00            103.60
  7            110.00            105.00
  ...
  ...
  26           250.00            250.00
```

```
*MISALIGNMENT TYPE
  2
*MISALIGNMENT
 10,10,26.0,26.0
```

Figure 8: Outline of unit cell with geometry points and fiber misalignment data points

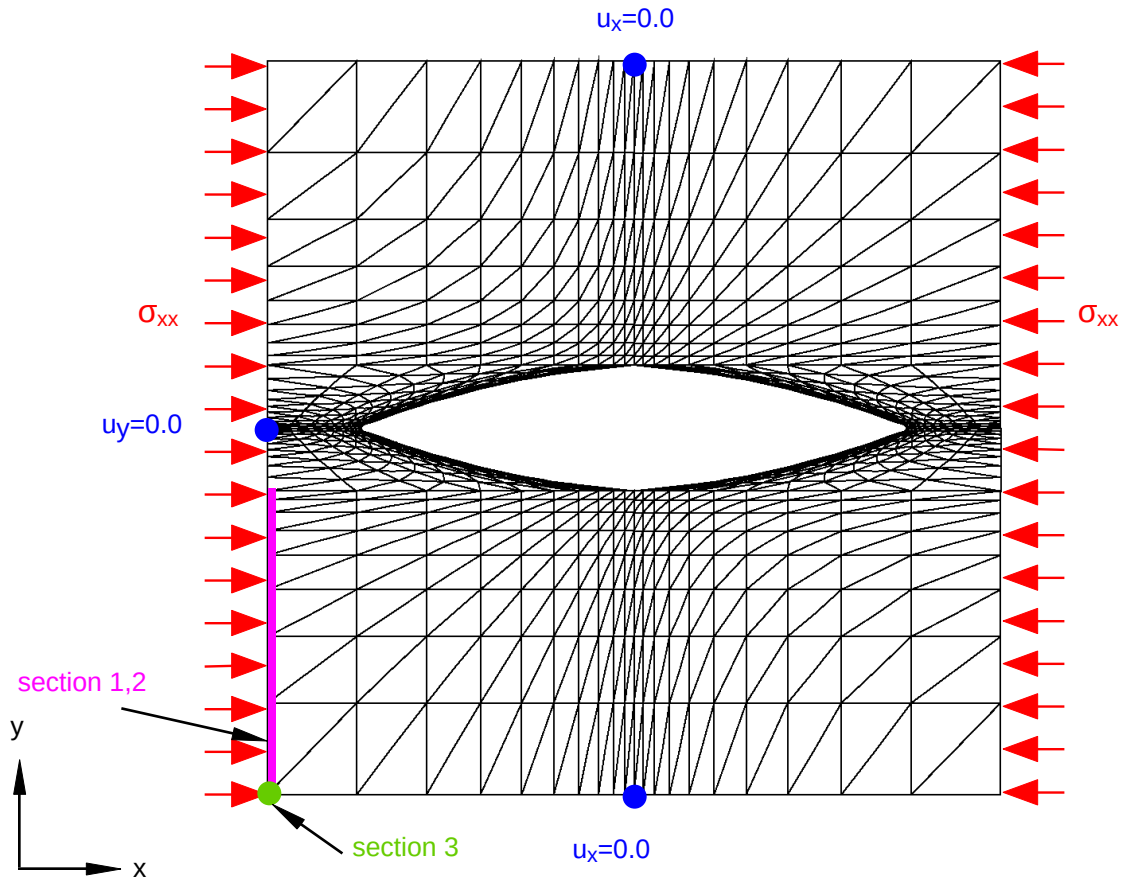


```
*STRESS LOADING
  10, 1
  1, 1, 4, 1, 1
  -1000, 0, 0, 0, 0
  4, 4, 9, 1, 1
  -1000, 0, 0, 0, 0
  9, 9, 15, 1, 1
  -1000, 0, 0, 0, 0
  15, 15, 21, 1, 1
  -1000, 0, 0, 0, 0
  21, 21, 24, 1, 1
  -1000, 0, 0, 0, 0
  3, 3, 6, 1, 1
  -1000, 0, 0, 0, 0
  6, 6, 12, 1, 1
  -1000, 0, 0, 0, 0
  12, 12, 18, 1, 1
  -1000, 0, 0, 0, 0
  18, 18, 23, 1, 1
  -1000, 0, 0, 0, 0
  23, 23, 26, 1, 1
  -1000, 0, 0, 0, 0
```

```
*TYPE 1 CONSTRAINTS
  3
  1, 1, 2, 21, 1, 1, 0
  9, 9, 15, 4, 4, 2, 0
  24, 24, 25, 21, 1, 1, 0
```

```
*OUTPUT LIST
  3
  1, 1, 4, 1, 1
  1, 1, 4, 1, 1
  1, 1, 4, 1, 17
```

Figure 9: Finite element model subjected to axial compression loading

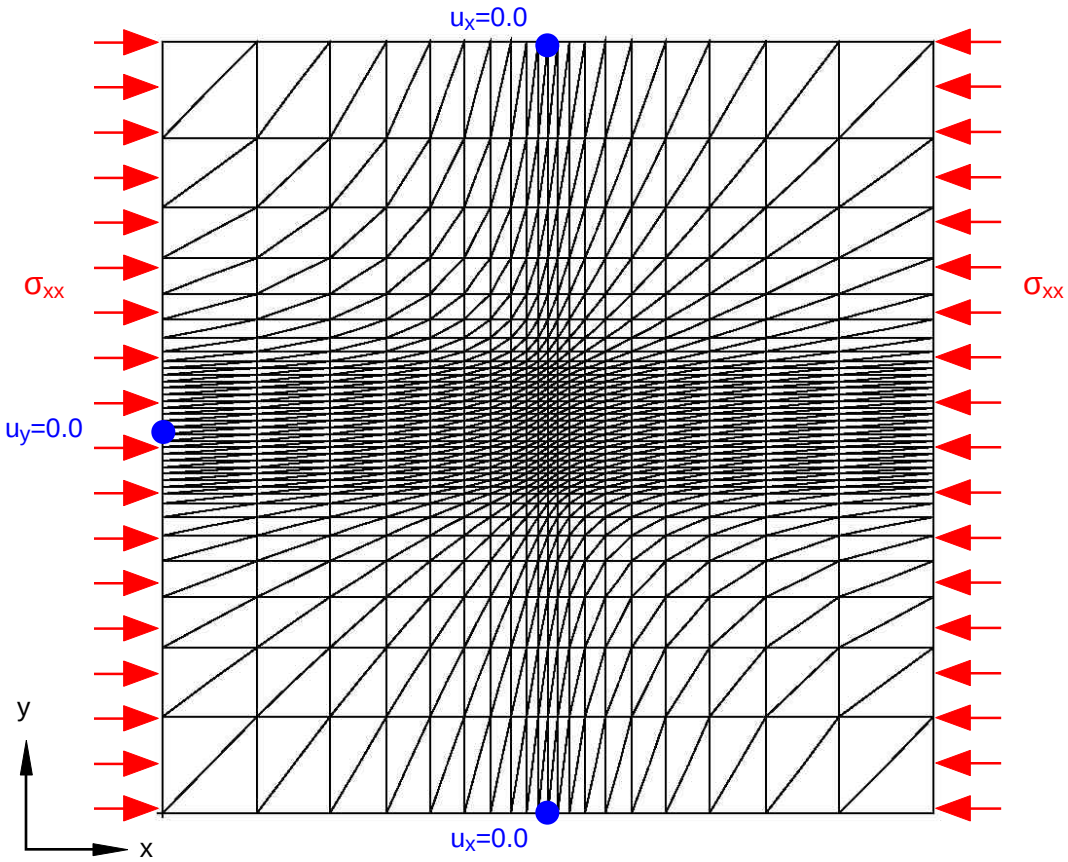

Figure 10: Mesh with axial compression load and boundary contions for UD Ply without Z-Pin

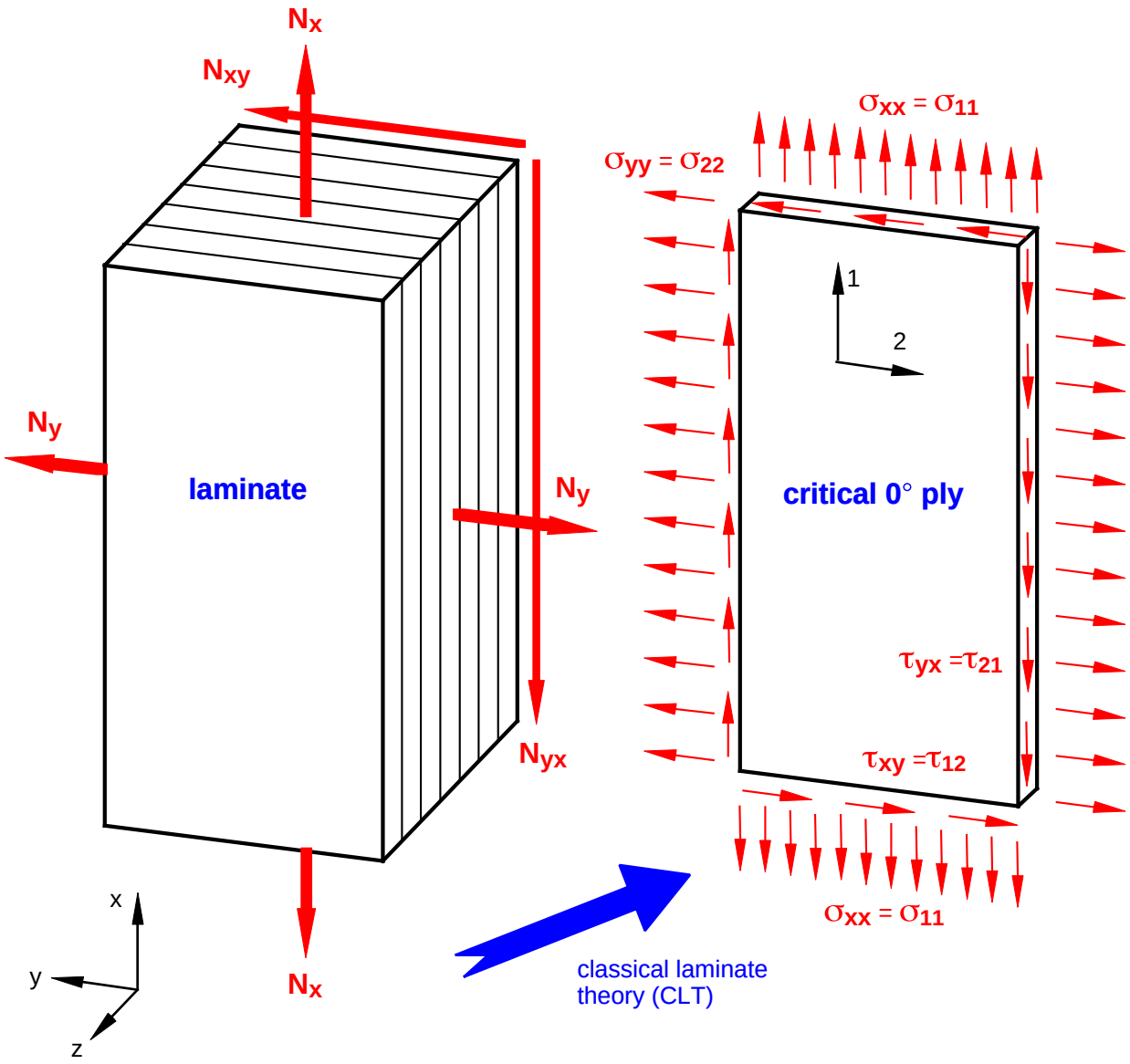

two load cases
N_x=1000 lbs/ in
N_x=1000 lbs/ in, N_{xy}= 1000 lbs/ in

three lamiantes
$[0/90]_s$
$[0/\pm45]_s$
$[0/45/-45/90]_s$

four critical cases identified
σ_{xx} (compression) only
σ_{xx} (compression), σ_{yy} (tension) = 2% σ_{xx}
σ_{xx} (compression), τ_{xy} = τ_{yx} =10% σ_{xx}
σ_{xx} (compression), τ_{xy} = τ_{yx} =10% $\sigma_{xx,}$, σ_{yy} (tension) = 2% σ_{xx}

Figure 11: Calculation of ply stresses using classical laminate theory

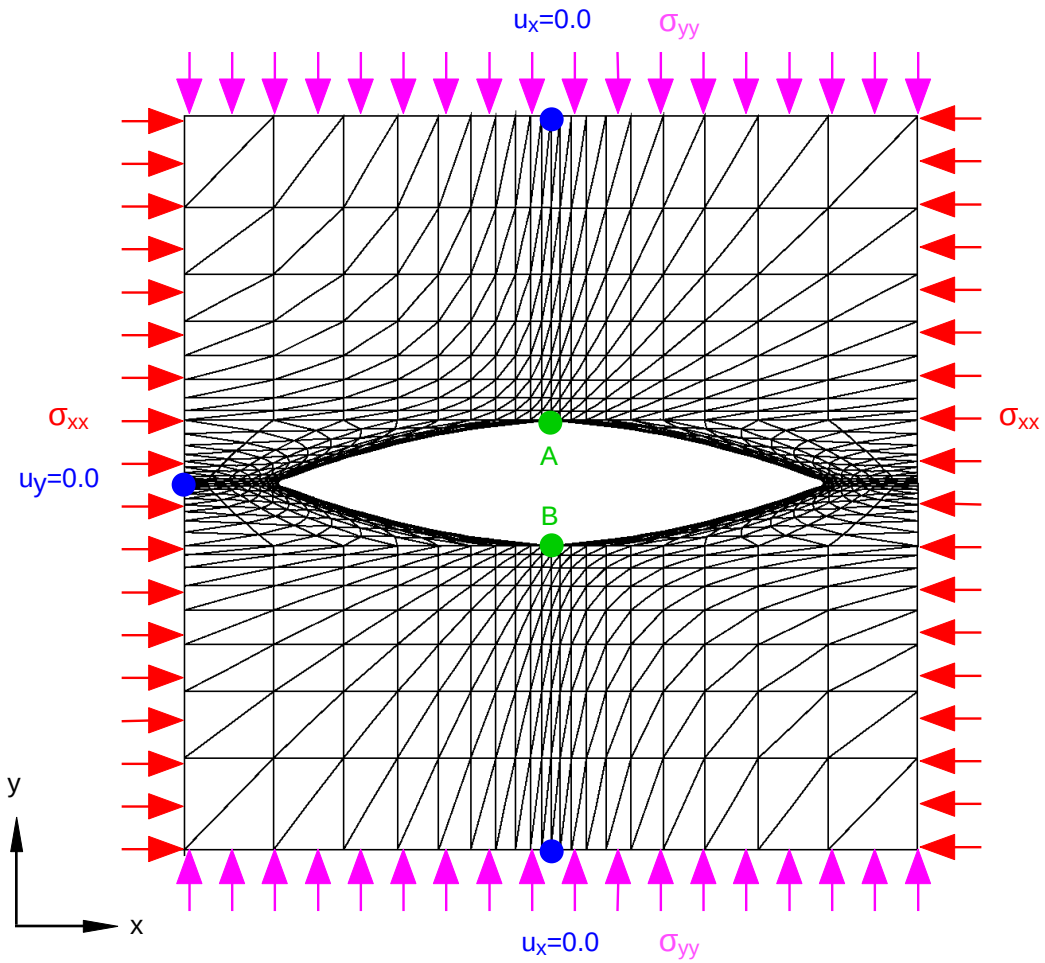


```
*STRESS LOADING
  14, 1
  1, 1, 4, 1, 1
  -1000, 0, 0, 0, 0
  4, 4, 9, 1, 1
  -1000, 0, 0, 0, 0
  9, 9, 15, 1, 1
  -1000, 0, 0, 0, 0
  ...
  ...
  23, 23, 26, 1, 1
  -1000, 0, 0, 0, 0
  1, 1, 2, 1, 1
  0, -20, 0, 0, 0
  2, 2, 3, 1, 1
  0, -20, 0, 0, 0
 24,24,25, 1, 1
  0, -20, 0, 0, 0
 25,25,26, 1, 1
  0, -20, 0, 0, 0
```

```
*TYPE 1 CONSTRAINTS
  3
  1, 1, 2, 21, 1, 1, 0
  9, 9, 15, 4, 4, 2, 0
  24, 24, 25, 21, 1, 1, 0
   5, 8, 11, 1, 17, 2, 0
  16, 19, 22, 17, 1, 2, 0
```

Figure 12: Finite element model subjected to axial and transverse compression loading

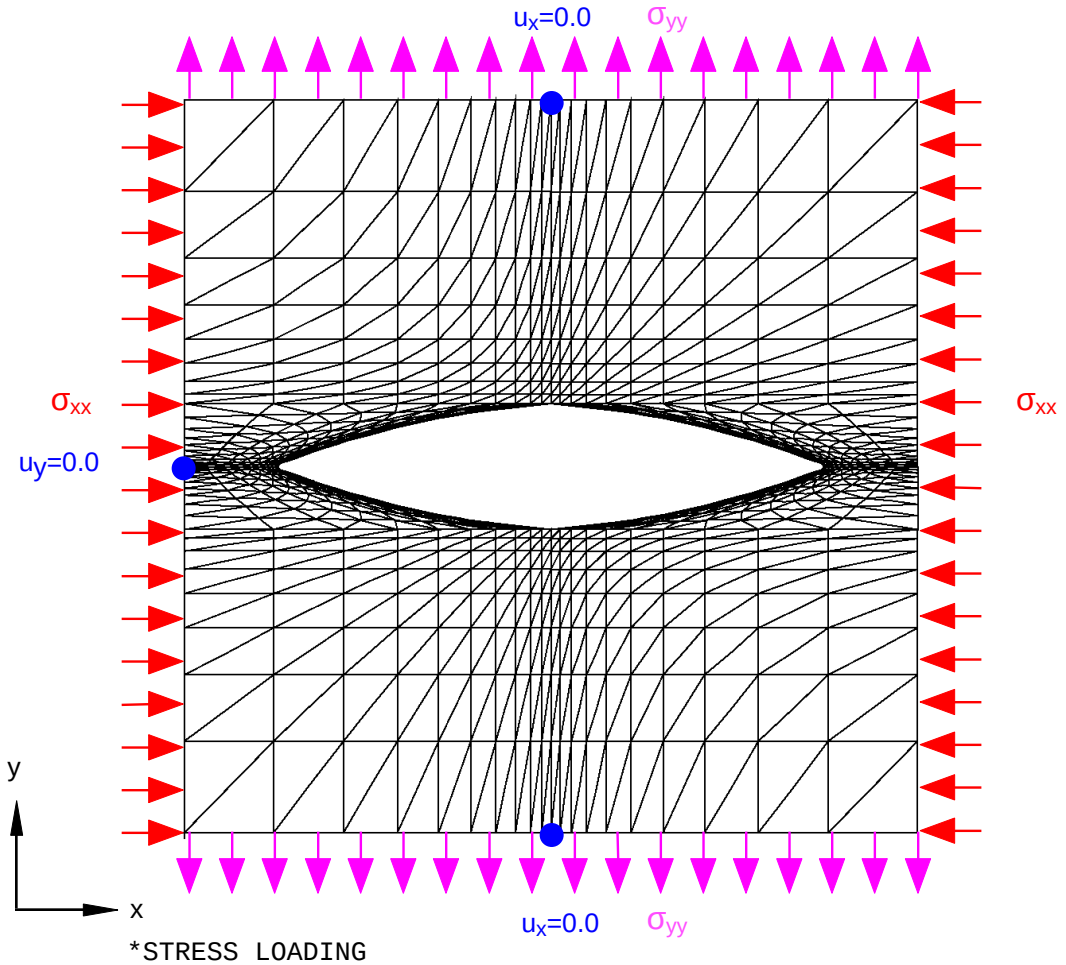


```
*STRESS LOADING
  14, 1
  1, 1, 4, 1, 1
  -1000, 0, 0, 0, 0
  4, 4, 9, 1, 1
  -1000, 0, 0, 0, 0
  9, 9, 15, 1, 1
  -1000, 0, 0, 0, 0
  15, 15, 21, 1, 1
  -1000, 0, 0, 0, 0
  ...
  ...
  23, 23, 26, 1, 1
  -1000, 0, 0, 0, 0
  1, 1, 2, 1, 1
  0, 20, 0, 0, 0
  2, 2, 3, 1, 1
  0, 20, 0, 0, 0
 24,24,25, 1, 1
  0, 20, 0, 0, 0
 25,25,26, 1, 1
  0, 20, 0, 0, 0
```

```
*TYPE 1 CONSTRAINTS
  3
  1, 1, 2, 21, 1, 1, 0
  9, 9, 15, 4, 4, 2, 0
  24, 24, 25, 21, 1, 1, 0
```

Figure 13: Finite element model subjected to axial compression and transverse tension loading

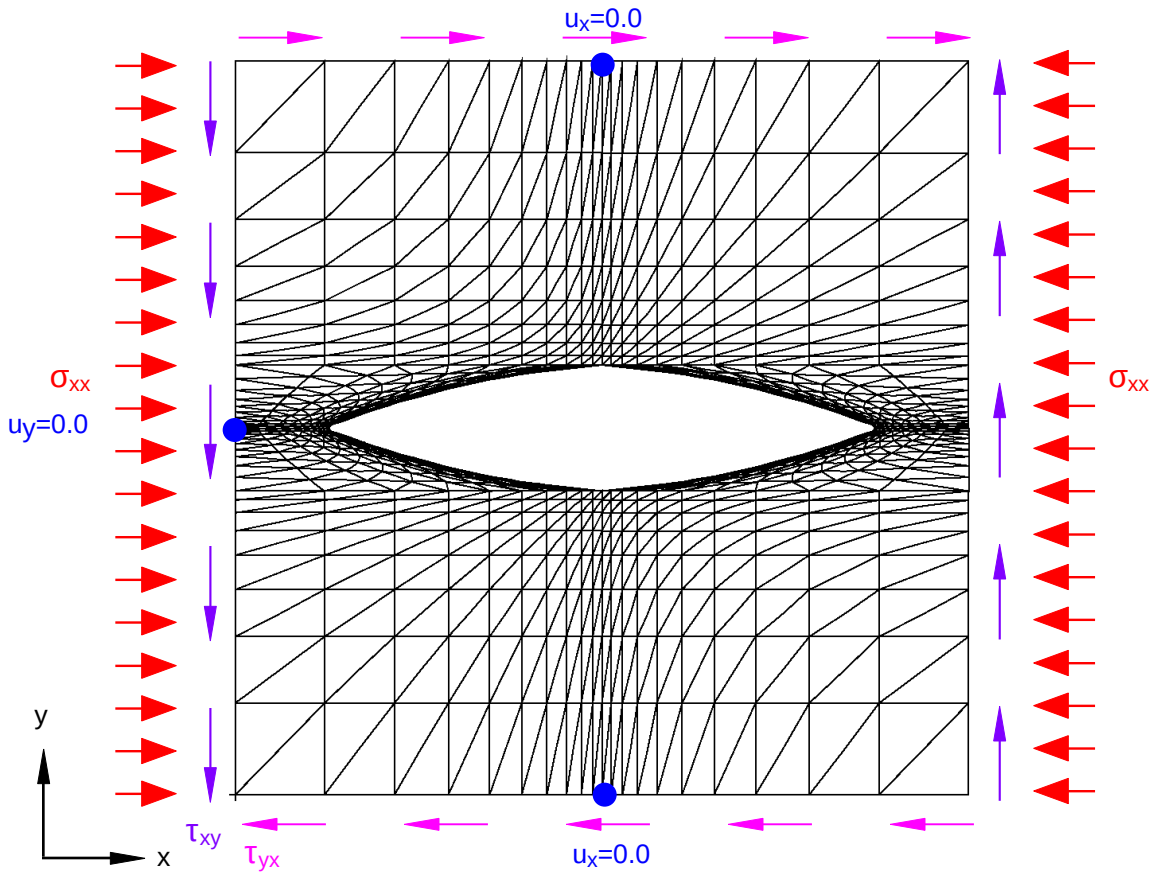


```
*STRESS LOADING
  14, 1
  1, 1, 4, 1, 1
  -1000, 0, -100, 0, 0
  4, 4, 9, 1, 1
  -1000, 0, -100, 0, 0
  9, 9, 15, 1, 1
  -1000, 0, -100, 0, 0
  15, 15, 21, 1, 1
  -1000, 0, -100, 0, 0
  ...
  ...
  23, 23, 26, 1, 1
  -1000, 0, -100, 0, 0
  1, 1, 2, 1, 1
  0, 0, 0, -100, 0
  2, 2, 3, 1, 1
  0, 0, 0, -100, 0
 24,24,25, 1, 1
  0, 0, 0, -100, 0
 25,25,26, 1, 1
  0, 0, 0, -100, 0
```

```
*TYPE 1 CONSTRAINTS
  3
  1, 1, 2, 21, 1, 1, 0
  9, 9, 15, 4, 4, 2, 0
  24, 24, 25, 21, 1, 1, 0
```

Figure 14: Finite element model subjected to axial compression and shear loading

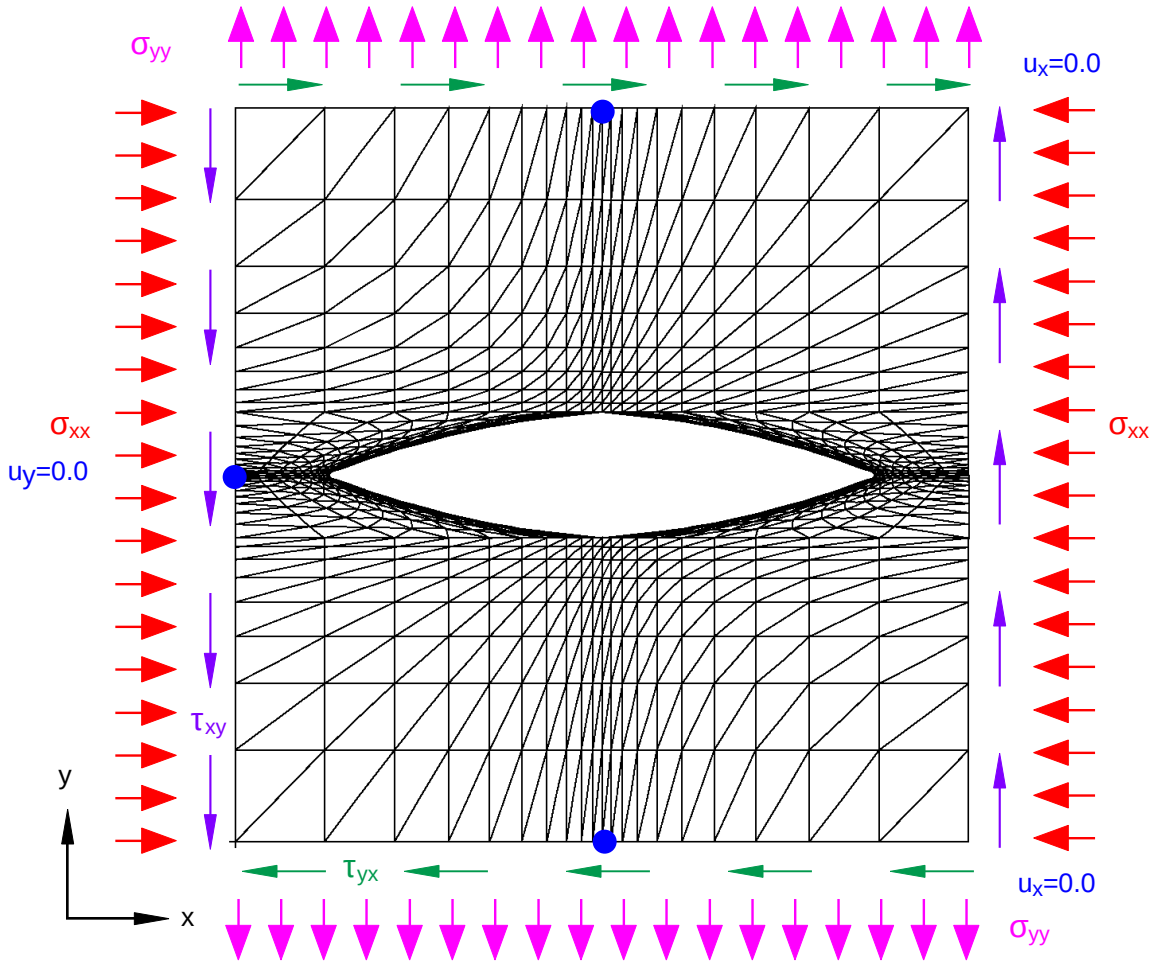


```
*STRESS LOADING
  14, 1
  1, 1, 4, 1, 1
  -1000, 0, -100, 0, 0
  4, 4, 9, 1, 1
  -1000, 0, -100, 0, 0
  9, 9, 15, 1, 1
  -1000, 0, -100, 0, 0
  15, 15, 21, 1, 1
  -1000, 0, -100, 0, 0
  ...
  ...
  23, 23, 26, 1, 1
  -1000, 0, -100, 0, 0
  1, 1, 2, 1, 1
  0, 20, 0, -100, 0
  2, 2, 3, 1, 1
  0, 20, 0, -100, 0
 24,24,25, 1, 1
  0, 20, 0, -100, 0
 25,25,26, 1, 1
  0, 20, 0, -100, 0
```

```
*TYPE 1 CONSTRAINTS
  3
  1, 1, 2, 21, 1, 1, 0
  9, 9, 15, 4, 4, 2, 0
  24, 24, 25, 21, 1, 1, 0
```

Figure 15: Finite element model subjected to compression, transverse tension and shear loading

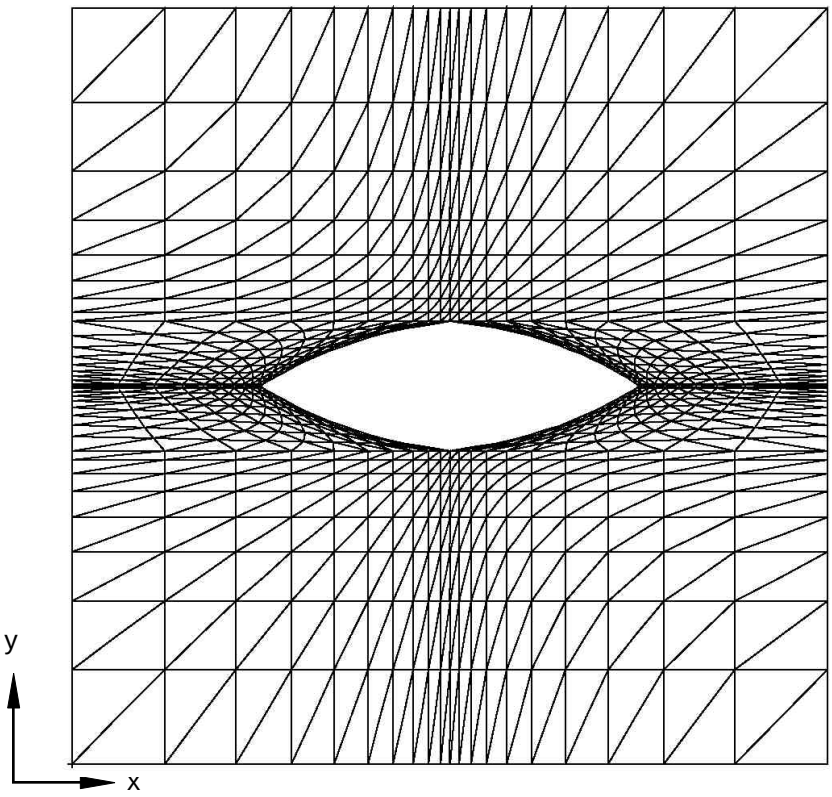

laminate with
2% carbon z-pins
C = 0.868 mm
D_z = 0.280 mm
D'_z = 0.3 mm
H_z = 1.7526 mm
L_z = 1.7526mm
d = 0.0051 mm

C /d = 170.2
D'_z /d = 58.8
H_z /d = 343.65
L_z /d = 343.65

```
*GEOMETRICAL POINTS
  26
  1              0.00              0.00
  2            171.85              0.00
  3            343.7               0.00
  4              0.00            142.45
  5            171.85            142.45
  6            343.7             142.45
  7            158.25            144.35
  8            185.75            144.35
  9              0.00            170.85
  10            86.75            170.85
  11           256.95            170.85
  12           343.7             170.85
  13            86.05            171.85
  14           257.65            171.85
  15             0.00            172.85
  16            86.75            172.85
  17           256.95            172.85
  18           343.7             172.85
  19           158.25            199.35
  20           187.75            199.35
  21             0.00            201.25
  22           171.85            201.25
  23           343.7             201.25
  24             0.00            343.7
  25           171.85            343.7
  26           343.7             343.7
```

```
*MISALIGNMENT TYPE
  2
*MISALIGNMENT
 74,74,4.7,4.7
```

Figure 16:Finite element mesh of unit cell for small z-pin with 2% areal density

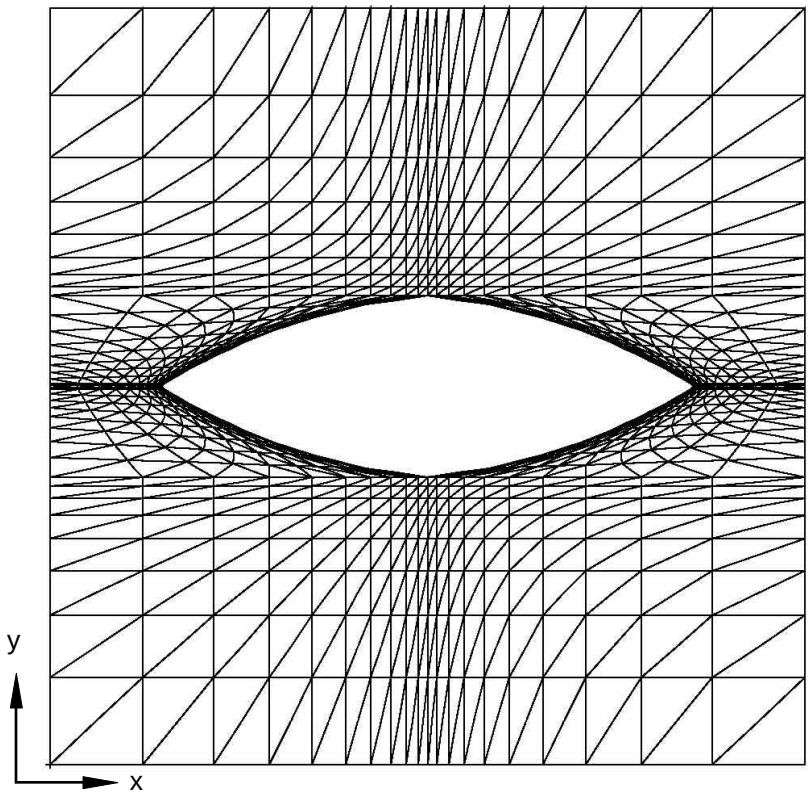

laminate with
4% carbon z-pins
C = 0.868 mm
D_z = 0.280 mm
D'_z = 0.3 mm
H_z = 1.2446 mm
L_z = 1.2446 mm
d = 0.0051 mm

C / d = 170.2
D'_z / d = 58.8
H_z / d = 244
L_z / d = 244

```
*GEOMETRICAL POINTS
  26
  1              0.00              0.00
  2            122.00              0.00
  3            244.00              0.00
  4              0.00             92.60
  5            122.00             92.60
  6            244.00             92.60
  7            108.10             94.50
  8            135.90             94.50
  9              0.00            121.00
  10            36.90            121.00
  11           207.10            121.00
  12           244.00            121.00
  13            36.20            122.00
  14           207.80            122.00
  15             0.00            123.00
  16            36.90            123.00
  17           207.10            123.00
  18           244.00            123.00
  19           108.10            149.50
  20           135.90            149.50
  21             0.00            151.40
  22           122.00            151.40
  23           244.00            151.40
  24             0.00            244.00
  25           122.00            244.00
  26           244.00            244.00
```

```
*MISALIGNMENT TYPE
  2
*MISALIGNMENT
 74,74,3.4,3.4
```

Figure 17:Finite element mesh of unit cell for small z-pin with 4% areal density

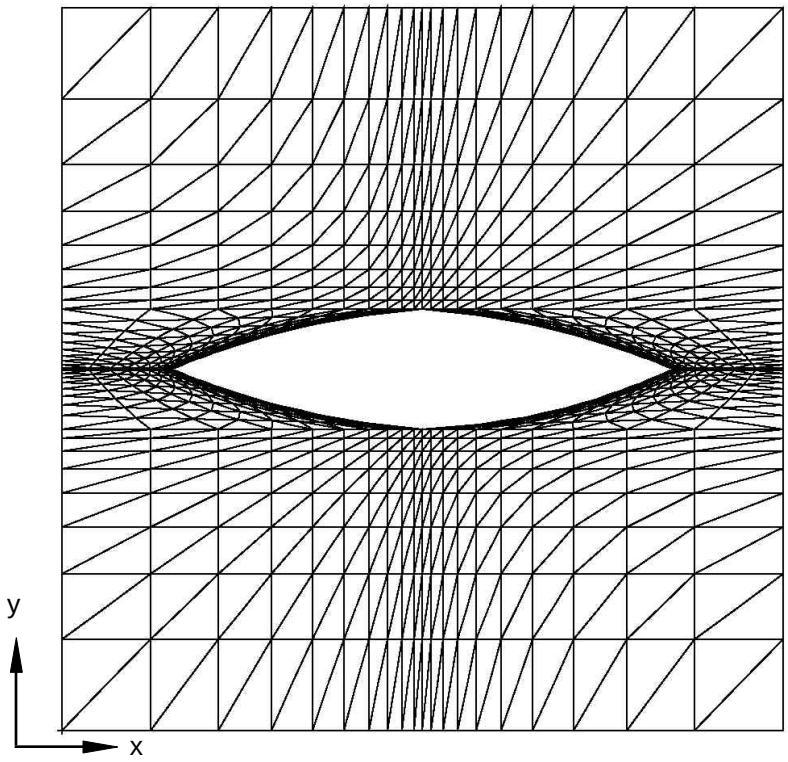

laminate with
2% carbon z-pins
C = 2.1844 mm
D_z = 0.508 mm
D'_z = 0.528 mm
H_z = 3.175 mm
L_z = 3.175 mm
d = 0.0051 mm

C / d = 428.31
D'_z / d = 103.53
H_z / d = 622.55
L_z / d = 622.55

```
*GEOMETRICAL POINTS
  26
  1              0.00              0.00
  2            311.275             0.00
  3            622.55              0.00
  4              0.00            259.51
  5            311.275           259.51
  6            622.55            259.51
  7            276.275           262.91
  8            346.275           261.91
  9              0.00            310.275
  10            97.12            310.275
  11           525.43            310.275
  12           622.55            310.275
  13            96.12            311.275
  14           526.43            311.275
  15             0.00            312.275
  16            97.12            312.275
  17           525.43            312.275
  18           622.55            312.275
  19           276.275           359.64
  20           346.275           359.64
  21             0.00            363.04
  22           311.275           363.04
  23           622.55            363.04
  24             0.00            622.55
  25           311.275           622.55
  26           622.55            622.55
```

```
*MISALIGNMENT TYPE
  2
*MISALIGNMENT
 74,74,8.6,8.6
```

Figure 18:Finite element mesh of unit cell for large z-pin with 2% areal density

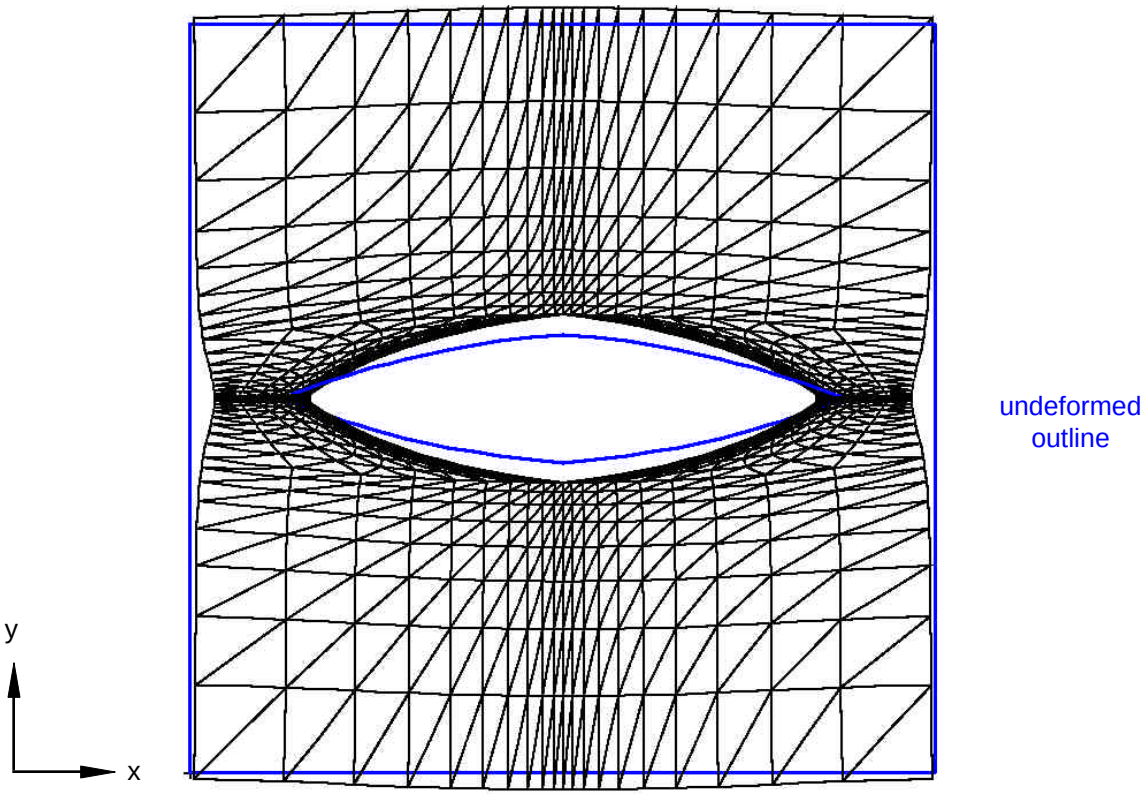

a. Deformed mesh after 10 load increments

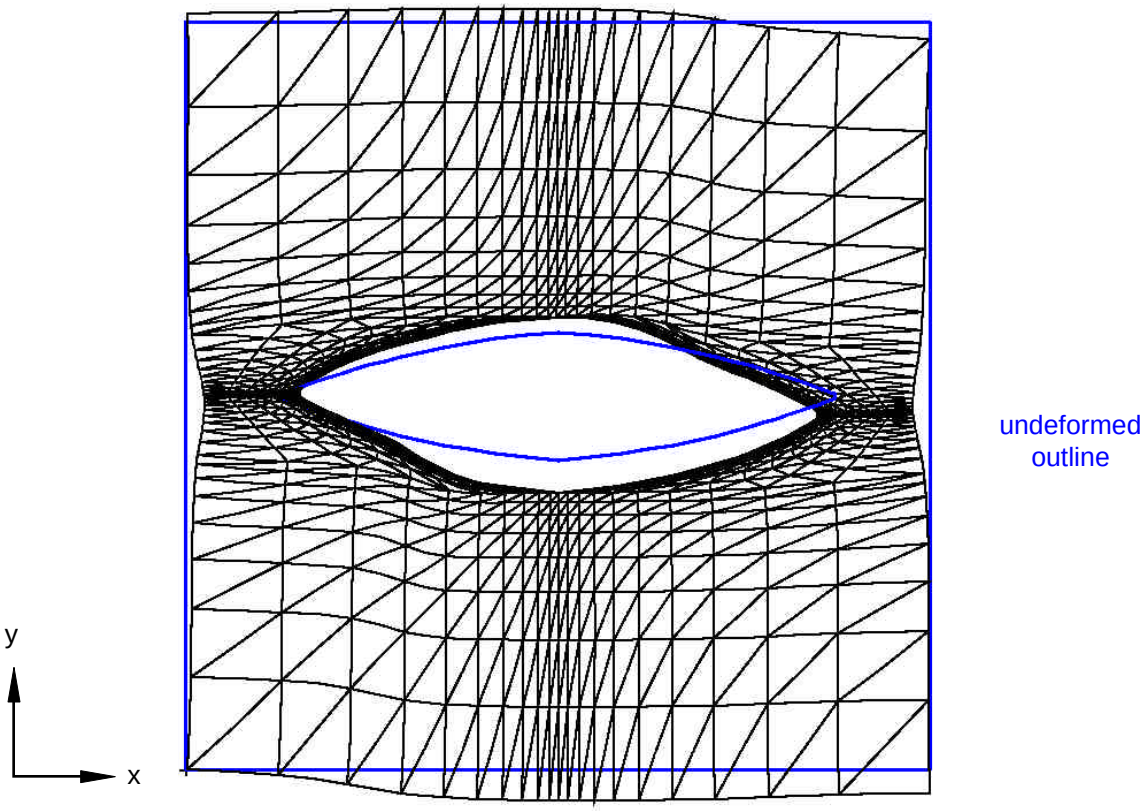

b. Deformed mesh after 1000 load increments

Figure 19: Analysis of unit cell of UD Ply with Z-Pin subjected to axial compression

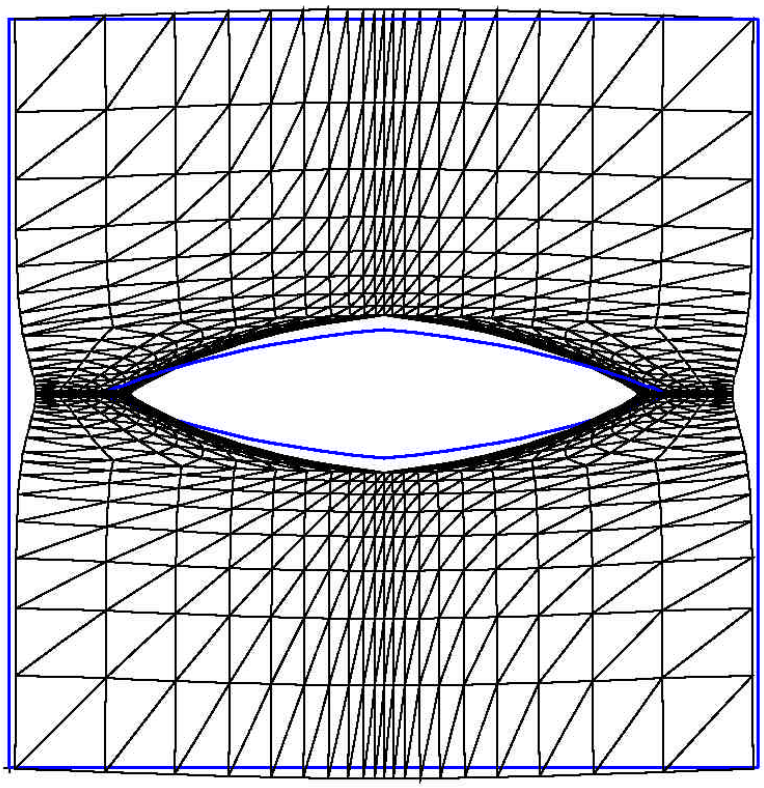

Figure 20: Deformed finite element model of unit cell subjected to axial and transverse compression loading

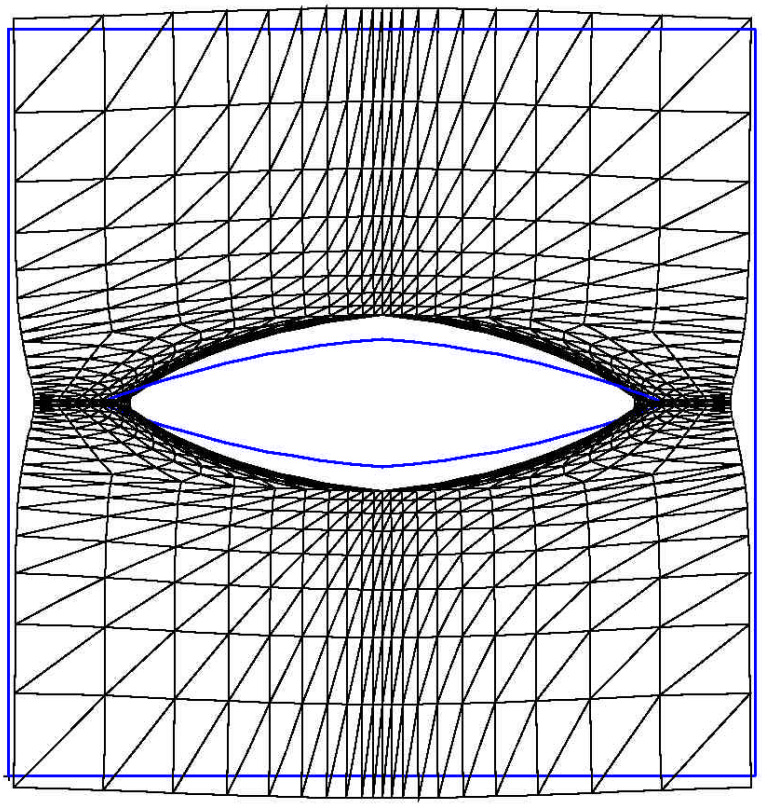

Figure 21: Deformed finite element model of unit cell subjected to axial compression and transverse tension loading

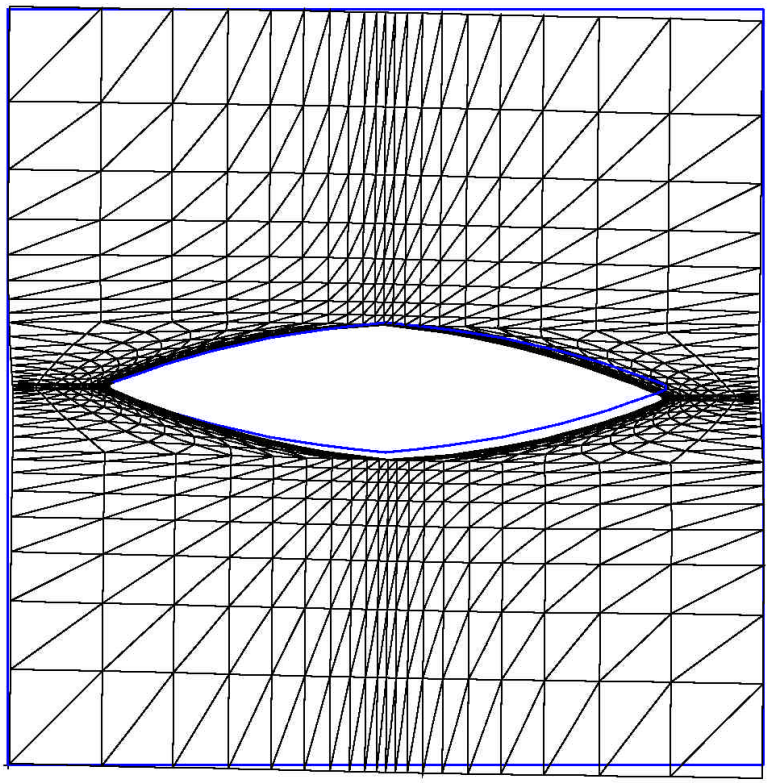

Figure 22: Deformed finite element model of unit cell subjected to axial compression and shear loading

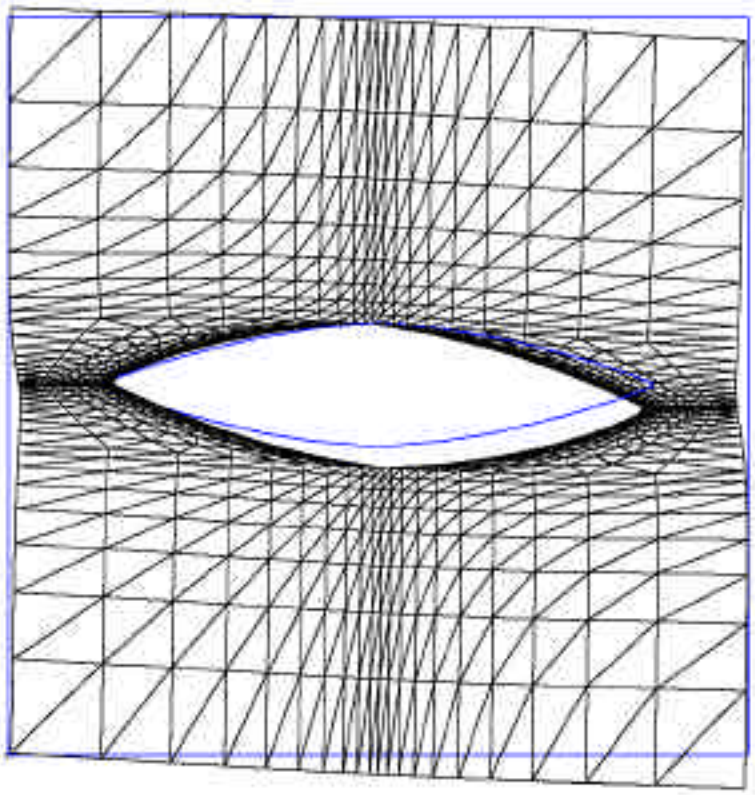

Figure 23: Deformed finite element model of unit cell subjected to axial compression, transverse tension and shear loading

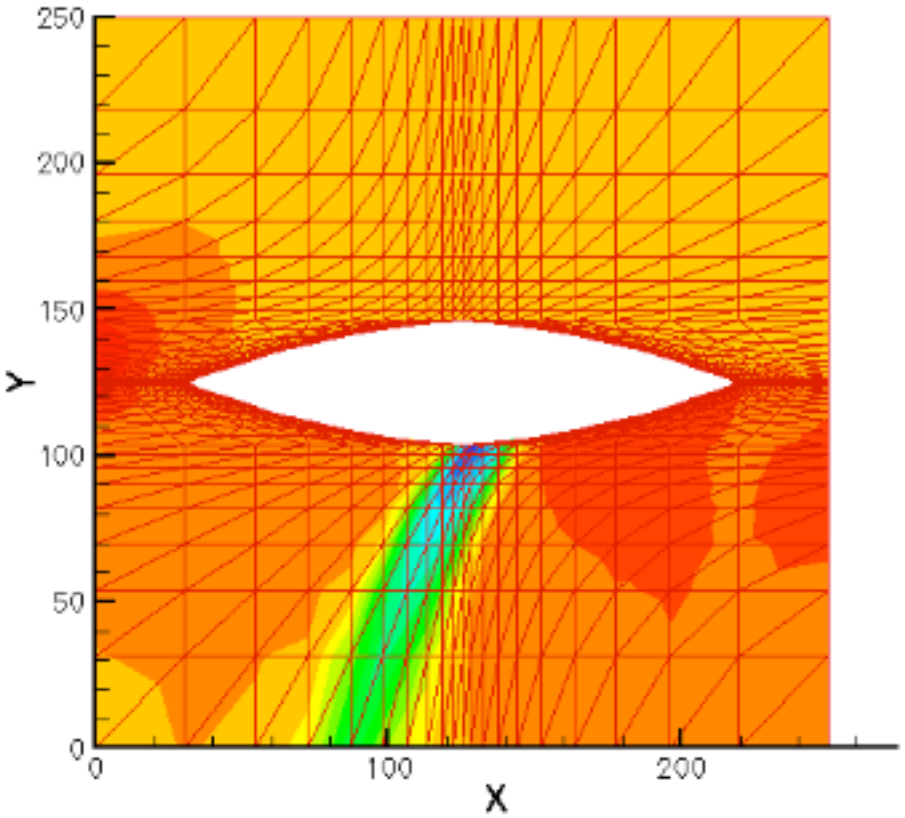

Figure 24: Contour plot of fiber misalignment angle ϕ

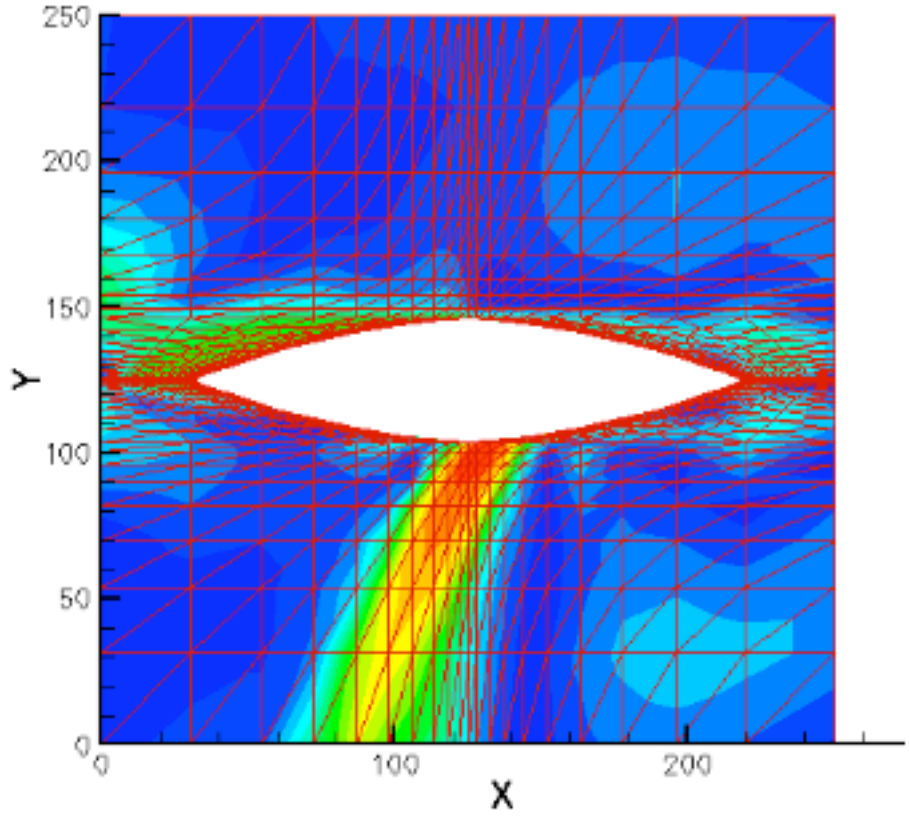

Figure 25: Contour plot of shear stress τ_e

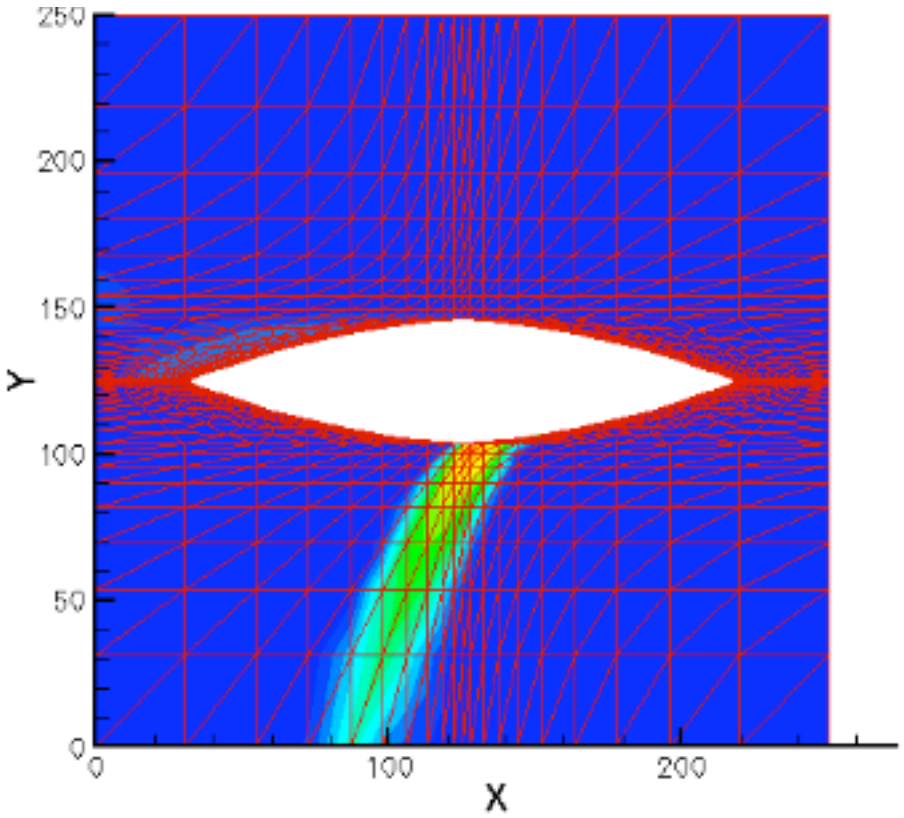

Figure 26: Contour plot of shear strain γ_p

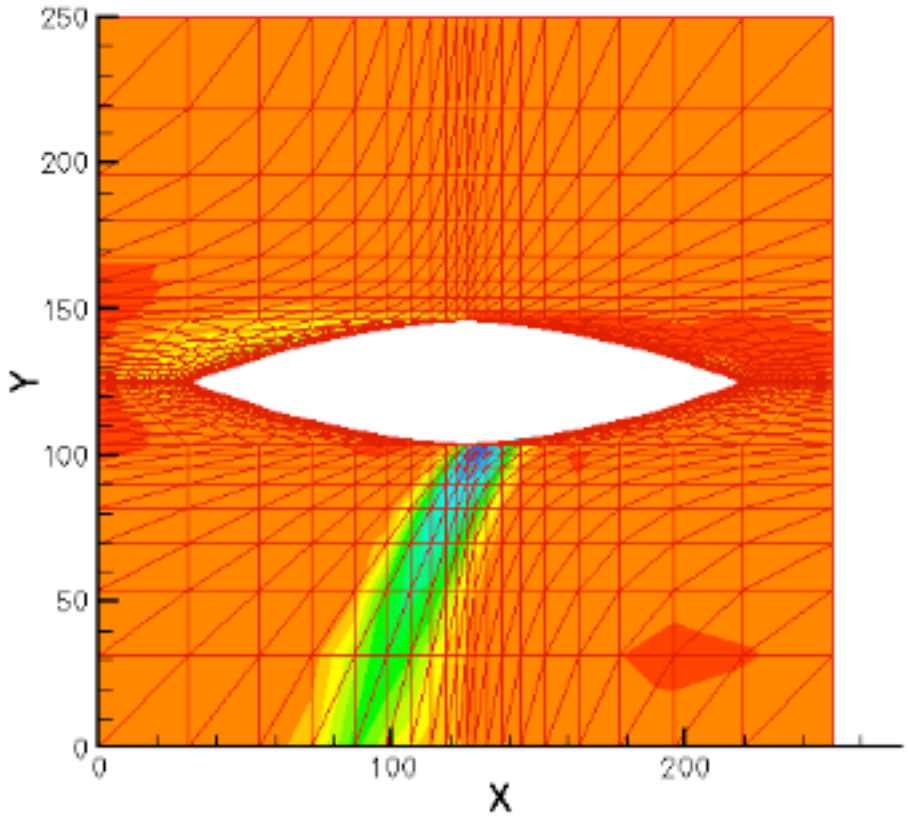

Figure 27: Contour plot of shear strain γ_s

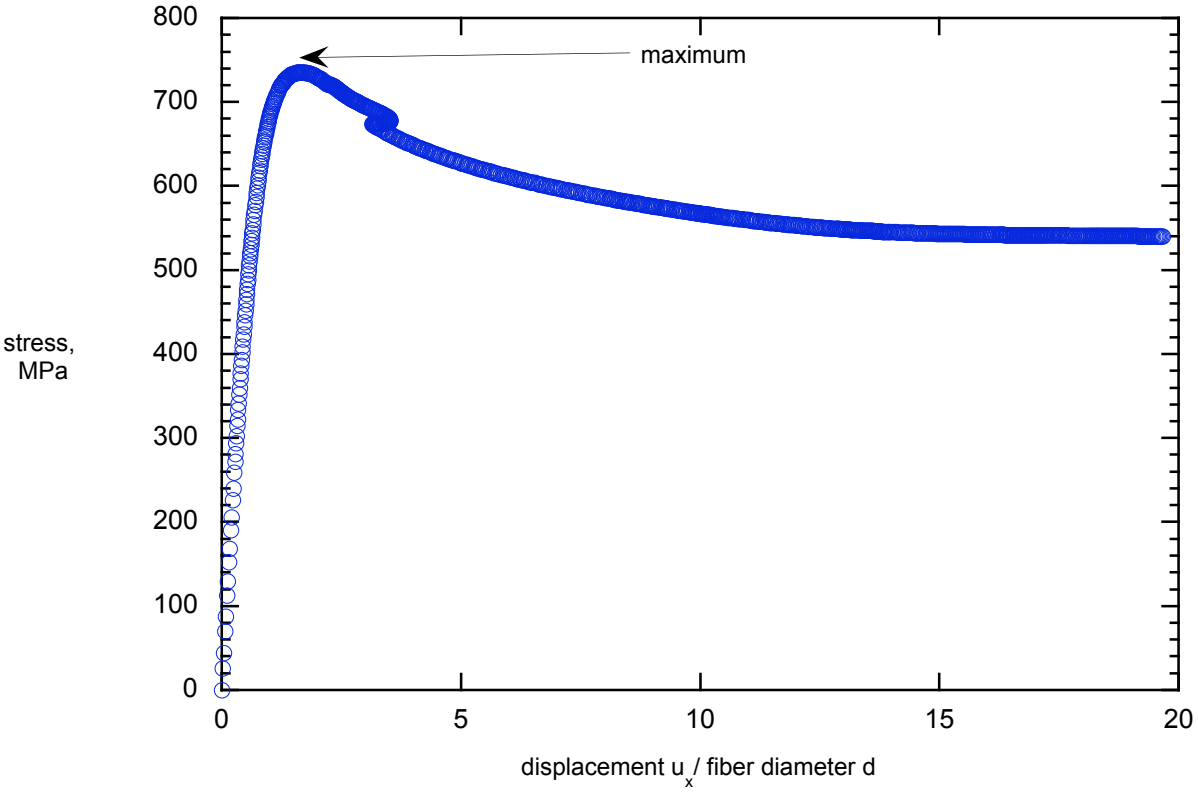

Figure 28. Stress-displacement plot

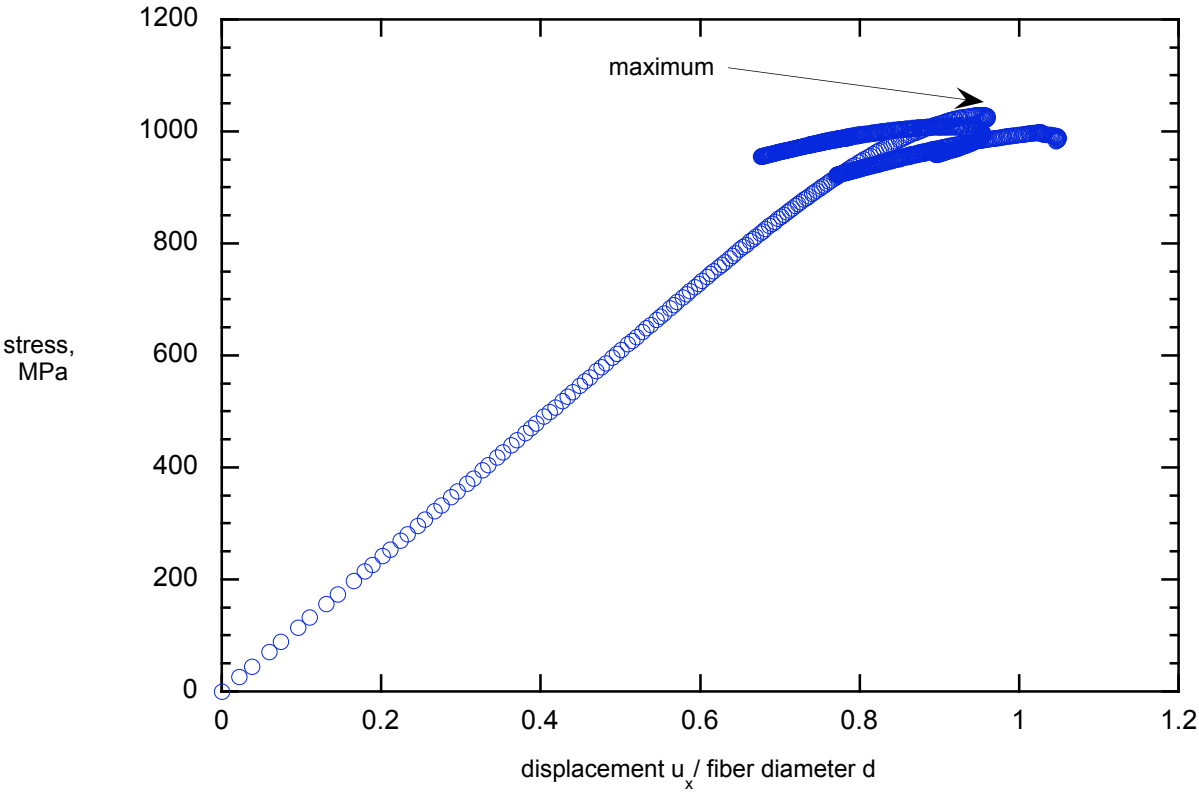

Figure 29. Stress-displacement plot

REPORT DOCUMENTATION PAGE

Form Approved
OMB No. 0704-0188

1. REPORT DATE *(DD-MM-YYYY)*	2. REPORT TYPE	3. DATES COVERED *(From - To)*
01/08/2005	Contractor Report	

4. TITLE AND SUBTITLE

Modeling of Unit-Cells with Z-Pins Using FLASH: Pre-Processing and Post-Processing

5a. CONTRACT NUMBER

NAS1-02117

5b. GRANT NUMBER

5c. PROGRAM ELEMENT NUMBER

6. AUTHOR(S)

Krueger, Ronald

5d. PROJECT NUMBER

5e. TASK NUMBER

1002

5f. WORK UNIT NUMBER

7. PERFORMING ORGANIZATION NAME(S) AND ADDRESS(ES)

NASA Langley Research Center
Hampton, VA 23681-2199

National Institute of Aerospace (NIA)
100 Exploration Way
Hampton, VA 23666

8. PERFORMING ORGANIZATION REPORT NUMBER

NIA Report No. 2005-01

9. SPONSORING/MONITORING AGENCY NAME(S) AND ADDRESS(ES)

National Aeronautics and Space Administration
Washington, DC 20546-0001

10. SPONSORING/MONITOR'S ACRONYM(S)

NASA

11. SPONSORING/MONITORING REPORT NUMBER

NASA/CR-2005-213905

12. DISTRIBUTION/AVAILABILITY STATEMENT

Unclassified - Unlimited
Subject Category 24
Availability: NASA CASI (301) 621-0390 Distribution: Nonstandard

13. SUPPLEMENTARY NOTES

Langley Technical Monitor: Tom Gates

14. ABSTRACT

Although the toughening properties of stitches, z-pins and similar structures have been studied extensively, investigations on the effect of z-pins on the in-plane properties of laminates are limited. A brief summary on the effect of z-pins on the in-plane tensile and compressive properties of composite laminates is presented together with a concise introduction into the finite element code FLASH. The remainder of the report illustrates the modeling aspect of unit cells with z-pins in FLASH and focuses on input and output data as well as post-processing of results.

15. SUBJECT TERMS

Composites; Z-Pinning; In-Plane Properties; Unit Cell; Finite Element Analysis; FLASH; Pre-Processing; Post-Processing

16. SECURITY CLASSIFICATION OF:			17. LIMITATION OF ABSTRACT	18. NUMBER OF PAGES	19b. NAME OF RESPONSIBLE PERSON
a. REPORT	b. ABSTRACT	c. THIS PAGE			STI Help Desk (email: help@sti.nasa.gov)
U	U	U	UU	49	19b. TELEPHONE NUMBER *(Include area code)* (301) 621-0390